Thesis for the degree of doctor of philosophy

Ocean Circulation in the Amundsen Sea, West Antarctica

Ola Kalén

UNIVERSITY OF GOTHENBURG

Doctoral Thesis

Department of Marine Sciences
Faculty of Science
University of Gothenburg

Gothenburg, Sweden, 2017

ISBN 978-91-629-0213-1 (Print)
ISBN 978-91-629-0214-8 (PDF)

Cover photo: Getz Ice Shelf, Amundsen Sea, Jan 9th 2014. Credit: Ola Kalén. All photos in this thesis by the author unless noted.

ola.kalen@marine.gu.se
Distribution: Department of Marine Sciences, University of Gothenburg

ISBN 978-91-629-0213-1 (Print)
ISBN 978-91-629-0214-8 (PDF)
Available at http://hdl.handle.net/2077/52056

Printed in Gothenburg, Sweden 2017 by Ineko AB

Abstract

The increase of mass loss from the Antarctic Ice Sheet is a significant contribution to global sea level rise. The most rapid changes are occurring in the Amundsen Sea area, where the thinning of the floating glaciers is assumed to be driven by the ocean. Relatively warm and salty deep water is forced upon the continental shelf and then flows southward in deep glacially scoured channels crossing the shelf. The warm waters contain enough heat to melt the glacial ice as they reach the base of the glaciers. The circulation of water masses on the Amundsen Sea shelf is sensitive to atmospheric forcing, while the regional atmospheric conditions are highly variable. A better understanding of this ice-ocean-atmosphere system is central to our ability to assess global sea level rise, which is occurring today and is projected to increase in the future.

The temporal variability, heat content, pathways and vertical structure of the ocean currents in primarily the Dotson-Getz trough, the main western pathway for warm deep waters on the Amundsen Sea continental shelf, were investigated in this study. The major data source for these analyses was in-situ subsurface moorings giving time series of temperature, salinity and current velocity. Other material includes shipborne measurements, numerical model output and a variety of satellite and reanalysis data. The main findings from this work are the following. In the bottom layer on the eastern side of the trough, there is a continuous inflow of warm deep water with a temperature of several degrees C above the local freezing point. The currents transporting the heat have a strong a depth independent part. Flow variability is substantial on daily and sub-daily timescales and inflows are correlated with regional eastward winds. The warm inflows interact with the base of the ice shelves and a part of this flow leaves the channel on the western side as cooled and freshened water mass. The assessed melt rates induced by this clockwise circulation agree with satellite based estimates. The bathymetry databases for this region contain large errors, which has implications for model studies and transport calculations.

Keywords: Antarctica, Amundsen Sea, West Antarctic Ice Sheet, Circumpolar Deep Water, shelf circulation, ocean model, icebergs, remote sensing

List of publications

This thesis is based on the following studies, referred to in the text by their Roman numerals. The published publications are reprinted with permission from the respective journals.

I. Wåhlin, A. K., O. Kalén, L. Arneborg, G. Björk, G. Carvajal, H. K. Ha, T. W. Kim , S. H. Lee, J. H. Lee, C. Stranne (2013) Variability of Warm Deep Water Inflow in a Submarine Trough on the Amundsen Sea Shelf. *Journal of Physical Oceanography*, 43, 2054 - 2010.

II. Ha, H. K., A. K. Wåhlin, T. W. Kim, S. H. Lee, J. H. Lee, H. J. Lee, C. S. Hong, L. Arneborg, G. Björk, O. Kalén (2014) Circulation and Modification of Warm Deep Water on the Central Amundsen Shelf. *Journal of Physical Oceanography*, 44, 1493 - 1501.

III. Wåhlin, A. K., O. Kalén, K. M. Assmann, E. Darelius, H. K. Ha, T. W. Kim , S. H. Lee (2016) Sub-inertial oscillations on the Amundsen Sea shelf, Antarctica. *Journal of Physical Oceanography*, 46.9 : 2573-2582.

IV. Kalén, O., K. M. Assmann, A. K. Wåhlin, H. K. Ha, T. W. Kim, S. H. Lee (2016) Is the oceanic heat flux on the central Amundsen sea shelf caused by barotropic or baroclinic currents? *Deep Sea Research Part II: Topical Studies in Oceanography*, *123*, 7-15.

V. Kalén, O., A. Mazur, A. K. Wåhlin, K. M. Assmann, T. W. Kim (2017) Iceberg drift as a proxy for upper ocean currents in the Amundsen Sea. *Submitted to Geophysical Research Letters.*

In Paper I, I had a major role in the data analysis task, writing the text and preparing several of the figures. For Paper II, my contribution was writing some of the text and discussing the conclusions. In paper III, I performed a large part of the data analysis, preparation of figures and the writing. During the work leading up to both paper IV and V, I had a principal role in formulating the research ideas, performing data analysis, writing and submitting the papers.

Peer reviewed publication not included in this thesis:

Stigebrandt, A., & O. Kalén, (2013). Improving oxygen conditions in the deeper parts of Bornholm Sea by pumped injection of winter water. *Ambio*, *42*(5), 587-595.

Table of contents

Part I

Summary

Knowledge speaks, but wisdom listens.

- Jimi Hendrix

1 Introduction

Antarctica is a land of extremes. This mythical "Terra Australis" (Southern Land) with its vast glaciers, ferocious seas dotted with icebergs and strange species found nowhere else, was the last region of earth to be discovered by humans. The first sighting of the mainland has been attributed to a Russian expedition in 1820, led by Fabian Gottlieb von Bellingshausen (Day, 2013), who now lends his name to one of the Antarctic marginal seas. It is the southernmost continent, to 98% covered by ice with an average thickness of 1.9 km (Fretwell et al., 2013), extending over all areas except the northernmost tip of the Antarctic Peninsula. Antarctica is on average the windiest, coldest and driest continent (Schwerdtfeger, 1984) with the highest mean elevation (Hastings et al., 1999). The continent covers about 10% of the land surface and holds 90% of the ice and 70% of the fresh water of the earth (Kennicutt et al., 2014). Antarctica is surrounded by the fourth largest ocean of the planet, the Southern Ocean, which is the central connection for the world ocean basins via the earth´s largest ocean current, the clockwise circulating Antarctic Circumpolar Current (ACC, Rintoul et al., 2001). The upwelling in the Southern Ocean is together with the North Atlantic down-welling the most important part of the global overturning circulation, which connects the deep and shallow layers of the ocean (Marshall & Speer, 2012). This makes the Southern Ocean disproportionately important to the climate and biogeochemistry of the earth relative to its size (Schofield et al., 2016).

The remoteness of this region, together with the extreme conditions of heavy sea ice, cold temperatures and high winds has always limited the number of scientific observations. But Antarctica and its surrounding ocean and atmosphere are today known to be experiencing fast changes. Regional disturbances such as loss of ice, changes in ocean circulation and atmospheric composition have global implications for sea level, climate, biodiversity and society. The oceans have absorbed an estimated 90% of the anthropogenically induced climate warming and thereby slowing the response to greenhouse gas forcing (Trenberth & Fasullo, 2013). The Southern Ocean has been responsible for more than 50% of this heat uptake during the last 50 years (Levitus et al., 2012), with the warming concentrated to the ACC (Gille, 2008; Gille et al., 2016). Half of the annual uptake of anthropogenic carbon from the atmosphere is taking place in the Southern Ocean (Le Quéré et al., 2007; Sallée et al., 2012). This rate of atmospheric drawdown of carbon has been hypothesized to have weakened (Sallée et al., 2012; Meredith et al., 2012). Changes have already been registered in various ecosystems (Smetacek and Nicol, 2005; Schofield et al., 2010). The ongoing

ocean acidification is predicted to continue quickly in the Southern Ocean, with substantial implications for its ecosystems (McNeil and Matear, 2008; Kawaguchi et al., 2013).

One key part of the Southern Ocean to understand these rapid changes is the Amundsen Sea, which up until the focused interest of the last decade has been the least sampled region. This is both due to the extreme conditions and the fact that no land based research station exists there and thus it has only been infrequently visited by research ships. This is the region where a large part of the West Antarctic Ice Sheet (WAIS) is drained into the ocean via its marine terminating outlet glaciers. The gravity driven discharge of ice from the continental ice sheet is now greater the mass added by precipitation over the interior, which results in a global sea level rise. Observations show that the Thwaites glacier is now losing mass at a rate of about 83 Gigatonnes yr^{-1} and may be in the first stages of a collapse with a potential to contribute to 1 mm yr^{-1} of sea level rise (Joughin et al., 2014; Scambos et al., 2017). The Getz ice shelf (Figure 1) is currently responsible for the largest part of the overall loss of ice from the Antarctic ice shelves, with a yearly average loss of approximately 54 Gt (Paolo et al., 2015). The rapid changes have significant implications for global sea level rise, a fact further emphasized by the possibility that the retreat of several of the glaciers may be irreversible (Rignot et al., 2014).

***Figure 1**. Getz ice shelf, Jan 2014.*

The melting of the West Antarctic glaciers is believed to be due to an increased heat supply from warm deep waters (Jenkins et al., 2010; Jacobs et al., 2011; Schmidtko et al., 2014). The warm and salty deep waters, originating from the ACC, access the floating parts of the ice sheets via deep troughs on the continental shelf and melt them from below. The first observations of ocean conditions on the continental shelf were presented by Jacobs et al. (1996) who found a presence of warm Circumpolar Deep Water (CDW) in Pine Island Bay. Today there exists a both spatially and temporally irregular collection of ocean measurements over 20 years helping to provide understanding of the system changes. The major aim of this thesis work is to add to the growing body of knowledge about the ocean forcing of the glaciological changes. Several important questions regarding the ocean circulation are not sufficiently resolved. How are the currents and their heat content changing over time? What paths do they take on the continental shelf? How much heat available for melting do they bring to the ice shelves?

This thesis is based on five papers that I have co-authored and then published or submitted to peer-reviewed scientific journals. The research work is summarized in the five chapters of the first part, where I have aimed to write the text in a simple way, such that a person with a general scientific interest can understand the basic significance of the results. The chapters are outlined as follows. A general description of the Amundsen Sea research area is given in chapter 2. The methods and material, including in-situ measurements, numerical modelling and satellite data, are explained in chapter 3. The most important results from the five papers are summarized in chapter 4. Finally, chapter 5 summarizes the main conclusions and a gives brief future perspective. The second part of the thesis shows the five research papers, which hold the complete details regarding my research.

2 Area description

2.1 Atmospheric conditions

The Amundsen Sea continental shelf area is characterized by fierce winds, heavy ice conditions and low temperatures, with above zero conditions occurring only sporadically during the austral summer. The atmospheric circulation is more variable than any other area on earth (Connolley, 1997), largely due to the movement and strength of the Amundsen Sea Low (ASL, Hosking et al., 2016), a climatological low pressure system approximately located between 60-180°W E and 60-80° S. The average longitudinal position of the ASL migrates from 110 to 150°W between austral summer and winter, influencing temperature, precipitation and winds. Variability in intensity and location of the ASL induce changes in ocean circulation as well as warm marine air intrusions (Nicolas & Bromwich, 2011). The ASL is strongly influenced by both tropical temperature changes connected to the El Niño-Southern Oscillation (ENSO, Ding et al., 2011) as well as the phase of the Southern Annular Mode (Marshall, 2003), an oscillation of air masses between high and mid latitudes which modulates the westerly winds.

***Figure 2**. Antipodean Albatross in a westerly gale, Amundsen Sea, Jan 2014.*

Time averaged (2006-2012) gridded fields of surface wind (Bumbaco et al., 2014), sea ice drift (Fowler et al., 2013) and sea ice concentration (Cavalieri et al., 1996) are shown in Figure 3. The surface winds are most intense over land, where catabatic winds are persistent, northwestward in the south and southwestward in the east. On the eastern side of the shelf area, winds are generally towards west, with decreasing intensity in the north closer to the shelf break. The western area of the shelf has winds of slightly larger magnitude, directed more towards northwest. North of the shelf break winds are generally very calm, this being the transition zone south of the large west wind belt beginning at 65°S.

The sea ice drift on the eastern part of the shelf tends to be directed towards north-northwest, to the right of the prevailing winds, with drift speeds increasing in the north at the shelf break. On the western shelf area, the drift direction is west to northwesterly and similar to the wind, with generally larger drift speeds than in the east. The time averaged sea ice concentration is consistently high over the whole shelf, except over the seasonal polynyas. The Amundsen polynya (Stammerjohn et al., 2015), north of Dotson ice shelf, and the area west of Pine Island glacier containing several smaller polynyas (Mankoff et al., 2012), have average concentrations between 0.3 and 0.4. The polynyas are biologically highly productive areas, also important for the distribution of sea ice (Randall-Goodwin et al., 2015).

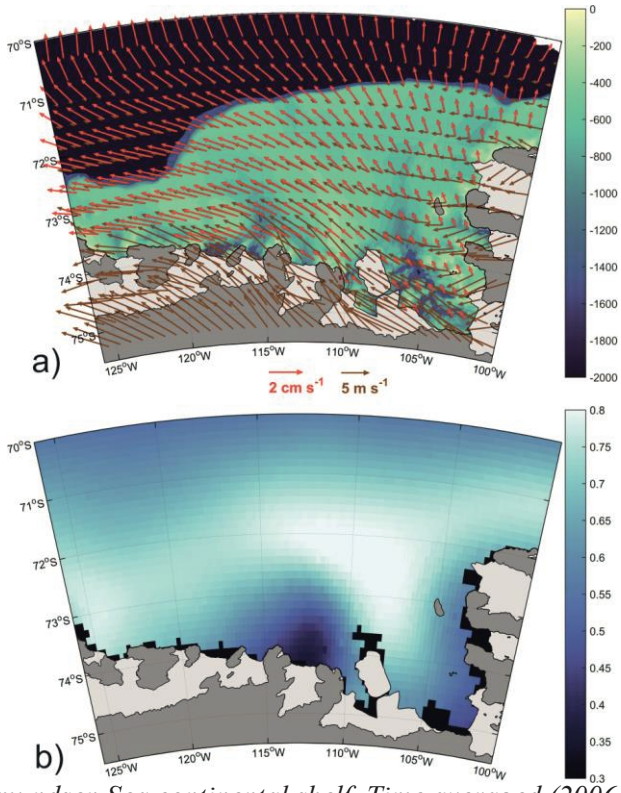

***Figure 3**. Amundsen Sea continental shelf. Time averaged (2006-2012) fields of **a)** surface winds (brown) and sea ice drift (red), **b)** Sea-ice concentration (fraction according to scale bar).*

2.2 Continental shelf and glaciers

The Amundsen Sea continental shelf (Figure 4) is cross cut by two major deep channels, carved by paleo-ice streams from past glacial epochs. These are the Dotson-Getz trough in the west and the Pine Island trough in the east. In the middle of the shelf, Pine Island trough bifurcates into a western and an eastern branch. The troughs reach the shelf break in the north, where depths drop rapidly from 500-600 m down to 2500 m. In the southern parts of the troughs, near the termination of the floating glaciers, there are basins with depths exceeding 1000 m. During the Last Glacial Maximum (Clark et al., 2009) about 23000-19000 years B.P., the WAIS reached further north onto the shelf, and may have extended all the way to the shelf break (Larter et al., 2014). The onset of the deglaciation has been dated to 14500 y B.P. (Larter et

al., 2014). The drivers for this glacial retreat are poorly constrained, but may include seafloor topography, global sea level rise and upwelling of warm water (Turner et al., 2017).

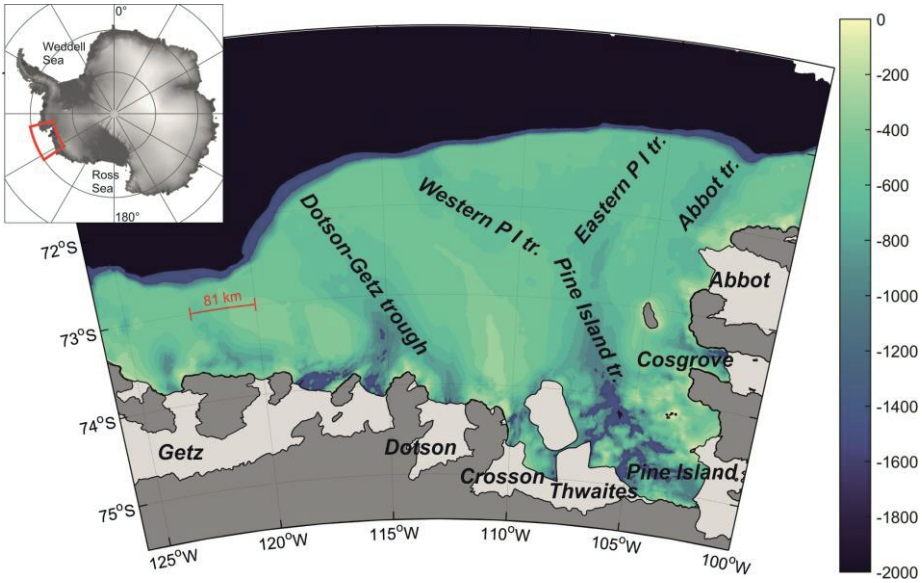

***Figure 4**. Map of Amundsen Sea continental shelf. Shown are major ice shelves and troughs. The bathymetry is from (Arndt et al., 2013).*

The outlet glaciers in the Amundsen Sea embayment have undergone rapid changes in recent decades. All glaciers in the area are fed by inland accumulation areas and the gravitationally forced flow of ice exits at the marine terminating floating ice shelves, which are grounded below sea level (Fretwell et al., 2013). The previously assumed approximate glaciological balance of the glaciers was questioned with the advent of surface elevation satellite measurements over the interior areas, beginning in the early 1990s (Jenkins et al., 2016). The glaciers have accelerated, thinned (Figure 5), retreated and been subject to basal melting by warm currents and currently contribute to approximately 10% of global sea level rise, with a future potential of 4.3 m for the whole WAIS (Turner et al, 2017; Fretwell et al., 2013). It has been found that the Thwaites glacier is undergoing the most rapid changes of any ice-ocean system in Antarctica (Paolo et al., 2015), now contributing to approximately 0.1 mm of sea level rise per year, twice as much compared with its mid-1990 rates (Scambos et al., 2017). The recent

growing research interest and urgency behind implications of future melting has provided thorough documentation of the changes, as summarized by Rignot et al. (2014) and Mouginot et al. (2014). In most locations around the continent, the accelerating melt rates are attributed to increased oceanic heat supply (Jenkins et al., 2010; Jacobs et al., 2011; Pritchard et al., 2012). Relatively warm Circumpolar Deep Water (CDW) access the underside of the floating ice shelves and melt them from below. This is in contrast to some other areas, such as the Larsen Ice Shelf, where warmer surface winds are thought to cause ice shelf disintegration (Doake et al., 1998).

2.3 Oceanographic conditions

Figure 5 shows an estimate of bottom water temperatures around the Antarctic continent (Orsi & Whitworth, 2005). Most parts of the continental shelves of East Antarctica and the eastern side of the Antarctic Peninsula are dominated by lower temperature waters, while in the Amundsen and Bellingshausen Seas and the western Antarctic Peninsula warmer waters are present. The waters on the continental shelves occupy a relatively narrow thermohaline range. Following Whitworth et al. (1998), they can be classified as follows: The upper layer consists of cold and fresh Antarctic Surface Water (AASW), which contains a cold core often termed Winter Water. Beneath the AASW is warm and salty Circumpolar Deep Water (CDW) and/or cold and salty Shelf Water (SW).

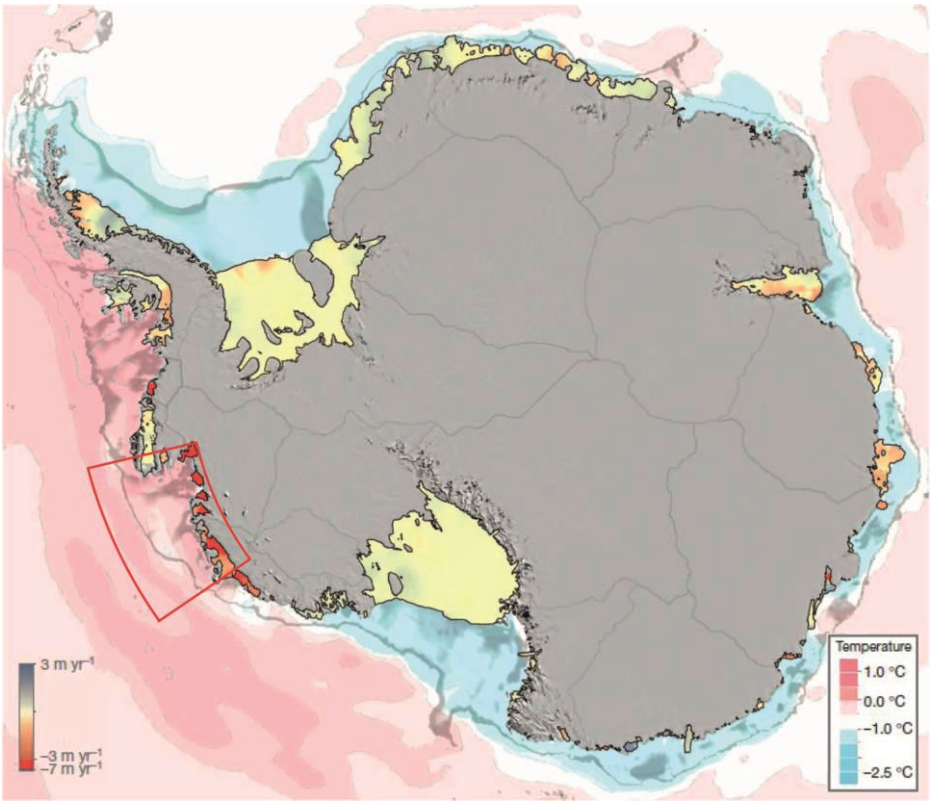

***Figure 5**. Rate of change of Antarctic ice-shelf thickness, 2003–2008 (according to left scale bar) and estimated average sea-floor potential temperatures (according to right scale bar) from the World Ocean Circulation Experiment Southern Ocean Atlas (Orsi & Whitworth, 2005). Image modified from figure 2 in Pritchard et al. (2012).*

The basal melting of the ice shelves is characterized by three modes (Jacobs et al., 1992; Jenkins et al., 2016). In Mode 1 melting, SW formed by brine rejection from sea ice formation enters below the ice shelves. The temperature of the SW is close to the in-situ freezing point, but still contains enough heat to melt the base of the ice shelves. This mode typically governs the slow melting on the largest ice shelves (Ross, Filchner-Ronne and Amery). Due to a large scale clockwise wind stress, the isotherms are depressed and the CDW layer is sloping downwards and cannot intrude on the shelf. In Mode 2 (Figure 6) CDW originating from the ACC enters the

base of the ice shelves after some modification. The low pressure systems giving clockwise wind patterns over the Amundsen and Bellingshausen Seas are centered over the continental shelf and the resulting weaker westward or even eastward winds cause an upward shoaling of the CDW layer which enhances deep water intrusions. Since the CDW can be up to 4°C warmer than the in-situ freezing point, the melting is fast and no SW can form. The mode 2 melting is highly sensitive to atmospheric variability due the associated vertical displacement of the pycnocline that separates the AASW and CDW waters (Heywood et al., 2016).

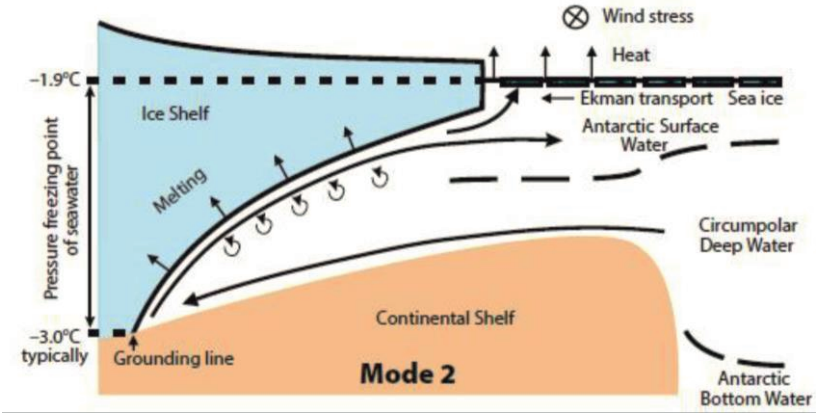

***Figure 6**. Mode 2 basal melt of an ice shelf and the associated circulation and stratification (Jacobs et al., 1992). Circumpolar Deep Water is the densest water on the shelf and no Shelf Water is present. Since CDW temperatures normally are around 3°C above the in situ freezing point, melting is rapid and no Shelf Water forms. Image modified from figure 3 in Jenkins et al. (2016).*

In Mode 3 melting, which occurs mainly at some smaller ice shelves in East Antarctica, AASW with temperature near the freezing point enters the ice shelf cavities. Melt rates are controlled by the cold core of the AASW and are similar to those of Mode 1, but an increased heat supply can be delivered by wind forced down-welling of the warmed upper layer AASW in summer (Hattermann et al., 2012). This thickening of the surface layer also acts to exclude the denser water masses below. These three regimes are governed by regional meteorological conditions, both via wind and snowfall and their influence on sea ice together with ocean dynamics and the proximity of the ACC.

The processes that control the warm inflows at the shelf break are not fully understood and their temporal variabilities need additional investigations (Heywood et al., 2016). Important mechanisms are thought to be wind forcing (Thoma et al., 2008; Wåhlin et al., 2013), bottom Ekman layer transport (Wåhlin et al., 2012) and a topographically steered eastward undercurrent (Walker et al., 2013; Assmann et al., 2013). High-resolution modeling studies have pointed to other alternatives, such as air-sea interactions in the polynyas (St-Laurent et al., 2015) as well as the location of the polynyas (Nakayama et al., 2014). The accelerated melting is determined by complex ocean-ice and atmosphere interactions, rather than a direct warming of the ocean. However, there are some indications that the waters of the ACC are getting warmer (Gille, 2008). A warming and shoaling of the CDW at the West Antarctic Peninsula and in the Amundsen and Bellingshausen Seas has been observed (Schmidtko et al., 2014), but in similarity with several others parts of the Southern Ocean, measurements remain sparse and are normally insufficient to confidently determine trends in longer term variabilities. The Amundsen Sea area is very sensitive to wind forced variabilities, partly due to the tropical Pacific teleconnections, thus decadal scale variability associated with ENSO and other climate oscillations may dominate other processes influencing oceanic changes on the shelf (Jenkins et al., 2016).

2.4 Icebergs

Icebergs are formed by calving at the fronts of marine terminating glaciers or by calving off other icebergs. They can have substantial impact on primary production (Smith et al., 2007; Biddle et al., 2015), local ocean circulation (Stern, 2015) and sea ice formation. During the drift of an iceberg, large quantities of freshwater are released into the upper ocean layer, an important component in the process of sea ice formation (Björk et al., 2002; Bintanja et al., 2015). This is evident in many parts of the Southern Ocean where melting icebergs are frequently surrounded by sea ice.

***Figure** 7. A tabular iceberg in the Amundsen Sea, Jan 2014.*

A map showing the probability of icebergs in the Amundsen Sea is given in Figure 8, using an iceberg database produced from radar satellite images by Mazur et al. (2017). The map shows the probability of finding an iceberg inside a grid cell (7.5 × 7.5 km). There are high probabilities of finding icebergs on top of shallow ridges and banks where they become stranded. Probabilities also coincide with depth contours in areas close to the iceberg sources at the ice shelf fronts. Locations of high likelihood are generally on the eastern side of ridges, indicating a westward drift of the icebergs over the shelf area. A large cluster of icebergs are stranded on the ridge separating the Dotson-Getz and Pine Island troughs. This acts as a barrier to the westward sea ice drift and strongly influences conditions in the Amundsen Sea polynya.

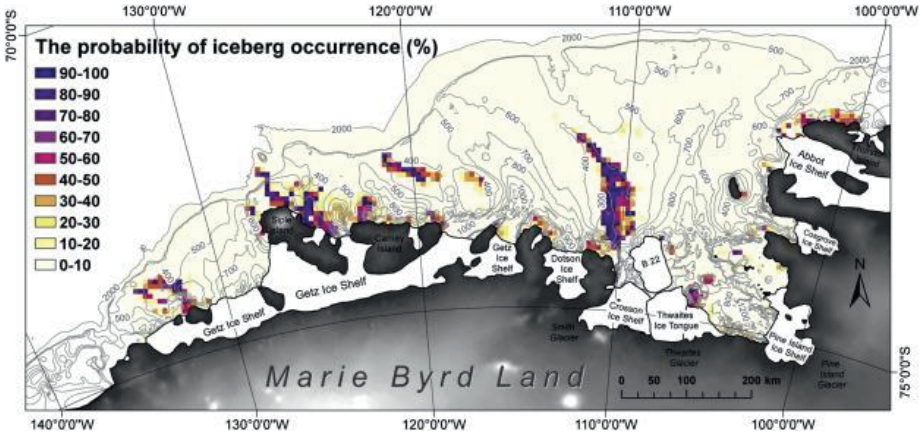

Figure 8. *Probability of occurrence of icebergs in the Amundsen Sea in 2011 (Mazur et al., 2017). Thin lines indicate bathymetry according to the IBCSO database (Arndt et al., 2013) and colors indicate iceberg probability by the ratio of the number of days that an iceberg is found to the number of days that have satellite image coverage.*

The annual mass loss from the glaciers terminating in the Amundsen Sea due to basal melt and calving during the recent decade has been approximated to 480 and 190 Gt year^{-1} respectively (Depoorter et al., 2013; Rignot et al., 2013). Thus it is probable that icebergs account for over a third of the ice budget. Despite indications that the Amundsen Sea is the most productive area in terms of iceberg mass (Liu et al., 2015), the knowledge about icebergs in this region is limited (Wesche & Dierking, 2015). There is a need for increased understanding of the ice-ocean interactions, including improved calving rate estimates, but also the fate of the icebergs after calving and their subsequent interactions with the ocean and atmosphere.

3 Methods

3.1 In-situ ocean measurements

Data from on-site hydrographic sampling are essential for understanding marine processes and form the basis of the research in this thesis. Two general methods were used, the stationary, bottom mounted mooring system (Figure 9) and the shipborne station work, where instruments are lowered from a ship (Figure 11), in our case an icebreaking research vessel. In both methods CTD (conductivity, temperature and depth) as well as current velocity sensors were used. The moorings provide the data continuous in time necessary for studying temporal variability while station data gives a spatial overview, although only during a snapshot in time.

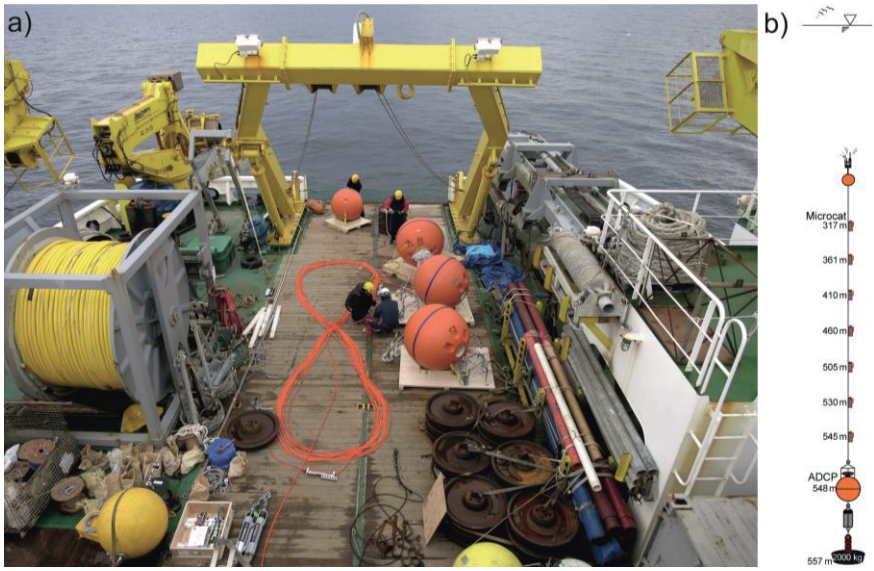

Figure 9 a) *A mooring deployment operation on RVIB Araon in the Amundsen Sea, Jan 2014.* ***b)*** *Sketch of a mooring setup (S1).*

The time series data used in this study are from six bottom mounted hydrographic moorings (Table 1, Figure 10), which were deployed and retrieved during austral summer cruises with the icebreakers RVIB Oden, RVIB Araon and RVIB Nathaniel B. Palmer. All moorings were equipped with arrays of CTDs (Seabird microCAT SBE37) to measure temperature and conductivity (from which salinity is derived). The accuracies are on the order of 10^{-3} K and 10^{-3} PSU (Practical Salinity Unit, Lewis & Perkin, 1981) respectively. For velocity measurements, the moorings S1 and S2 were both equipped with a 150 kHz Quarter Master Acoustic Current Doppler Profiler (ADCP, RD instruments). This upward looking instrument transmits a fixed frequency pulse and uses the Doppler shift of the echo returning from sound scatterers, mostly zooplankton with size of around 1 mm, assumed to move with the same velocity as the currents. In the clear waters on the Amundsen Sea shelf, the depth range will normally be 200-250 meters with a velocity resolution on the order of 10^{-1} cm s^{-1} for a 150 kHz ADCP.

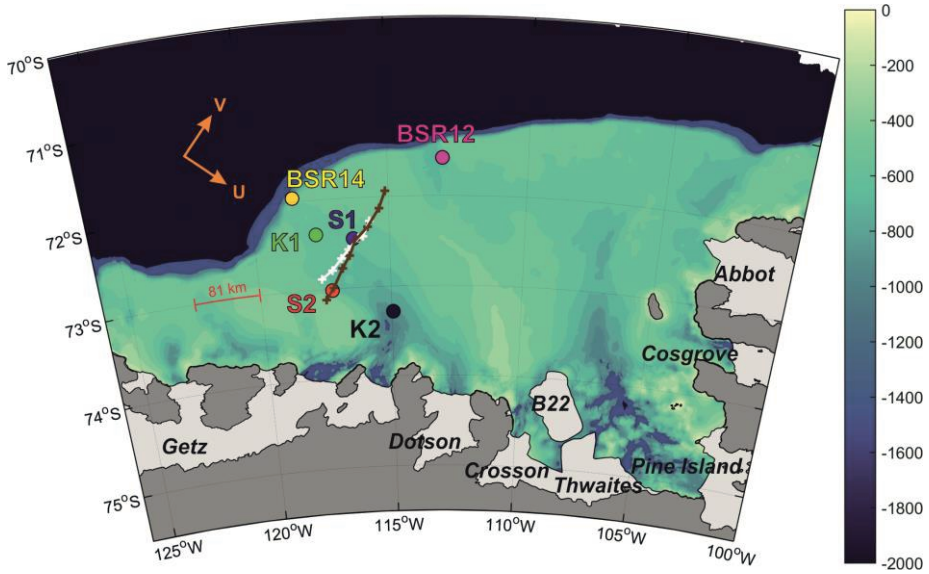

Figure 10. *Map of Amundsen Sea continental shelf. Shown are mooring positions (colored circles), major ice shelves, two cross-trough sections (brown 2010, white 2008), geometry of channel rotated velocities (orange arrows) and iceberg B22 (approximate outline and position in Jan 2012). The bathymetry is from the IBCSO database (Arndt et al., 2013).*

***Table 1**. Coordinates, depths and instrumentation type for bottom mounted moorings.*

Mooring	Long W	Lat S	Bot. Dep. (m)	Sensor types	Used in Paper
S1	116.349	72.455	557	ADCP/CTD	I-V
S2	117.249	73.017	546	ADCP/CTD	II-V
K1	117.710	72.387	253	Current meter/CTD	II, V
K2	114.950	73.281	275	Current meter/CTD	II,V
BSR12	113.042	71.576	611	Current meter/CTD	V
BSR14	118.463	71.959	602	Current meter/CTD	V

The moorings K1and K2 were fitted with several RCM-11 current meters (Aanderaa). This is also an acoustic Doppler instrument, but one which transmits horizontal beams and thus measures currents at one discrete depth with velocity resolution of 10^{-1} cm s^{-1}. BSR12 and BSR14 were equipped with AEM-USB current meters (Alec Electronics), which are electromagnetic velocity meters. Velocity, at the depth of the instrument only, is deduced from the potential differences between the electrodes as the water flows through the magnetic field generated by the instrument, with a resolution of 10^{-2} cm s^{-1}.

Tides can be significant in coastal regions and it is often necessary to separate the tidal and non-tidal signal when analyzing ocean time series. Tides play an important role also in the Antarctic coastal Seas, with the strongest tides found in the Weddell Sea where they can generate mean currents of up to 5 cm s^{-1} and have a large impact on ice shelf melting (Mueller et al., 2012). Tides are weaker in the Amundsen Sea, but may still have a significant impact for circulation and melting under the ice shelves (Robertson, 2013). For the mooring time series, de-tiding can be carried out with harmonic analysis, where the tidal signal is modeled as a sum of individual oscillations at frequencies connected to astronomical parameters. The Matlab t_tide package (Pawlowicz et al., 2002) was used to de-tide all time series.

For the shipborne stations, a rosette, including water samplers, a CTD (Sebird 911+) and a downward looking lowered ADCP (LADCP) was used (Figure 11). The LADCP data were then processed to correct for instrument and ship motions and to transform the relative current profiles to a fixed reference, here the inversion method developed by Visbeck (2001) was used. For tidal prediction at such stations lacking the temporal resolution, a model is needed. For this purpose, the The Circum-Antarctic Tidal Simulation (CATS, Padman et al., 2002) was utilized, which is an inverse model constrained by data assimilation widely used in the Southern Ocean.

Figure 11*. A rosette, including CTD and LADCP, lowered from RVIB Araon in the Amundsen Sea, Jan 2014. Getz ice shelf in the background.*

The quality control threshold in the processing of the ADCP data was error velocity below 15 cm s^{-1} and correlation magnitude values greater than 110 for at least three of the four beams. In paper V, it was of interest to get the uppermost velocities from the ADCP since connections between icebergs and

currents were investigated. From the data which passed the quality control, the 10 shallowest bins (each 8 meter deep) at each time were chosen. At mooring S1, the uppermost measurements varied between 201 and 481 m with standard deviation 33 m. Currents were then averaged over the 10 top bins with the resulting average depth of 314 m for the whole measurement period. The same procedure was applied to the S2 data, with top measurement depth varying between 213 and 437 m (st. dev. 40 m) and the average 10 bin depth of 314 m.

3.2 Circulation model

In-situ measurements in the polar oceans remain difficult and expensive, using icebreakers in remote areas with heavy sea ice. During the past several decades, numerical models have been an increasingly important tool to study how oceans are interacting with the ice shelves, contributing both to process understanding and increase in data coverage. Necessary physical processes to resolve in simulations are melting at the ice-ocean interface, circulation in the ice shelf cavities and the oceanic heat transport from the open ocean (Dinniman et al., 2016). Despite great progress both in system knowledge and computational power, it is currently not possible to fully simulate the complex interactions between the surface atmospheric flow, the oceanic conditions and the ice shelf dynamics in the models. This is in part due to lack of resolution of topographic and bathymetric features and limited knowledge of sub-ice shelf conditions (Turner et al., 2017) and a shortage of observations against which to compare and test the models and use as boundary conditions.

The model data used in paper IV and V were from a regional setup of MITgcm (Marshall et al., 1997), which is an open-source 3D, z-coordinate ocean circulation model. It was previously applied to investigate deep water intrusions on the shelf by Assmann et al. (2013), whose study the reader is referred to for further information.

The model setup includes a sea ice model (Losch et al., 2010) and a sub-ice shelf-ocean interaction model (Losch, 2008) applied on the domain 80°-140°W and 62-76°S. The resolution is 0.1° longitude and 0.1° x cos (φ) latitude, which corresponds to an average of 3.3 km over the shelf. The initial conditions came from World Ocean Atlas (WOA) 2009 salinity (Antonov et al., 2010) and potential temperature (Locarnini et al., 2010). The model was forced with atmospheric data from the National Centers for Environmental

Prediction Climate Forecast System Reanalysis (NCEP CSFR) as described by Saha et al. (2010). The bathymetry and ice shelf topography is from the RTOPO1.0.5 dataset (Timmermann et al., 2010). The model has 50 vertical layers, of which 20 are located in the upper 1000 m. Monthly averages from WOA09 were used to prescribe salinity and potential temperature at the open boundaries. The boundary conditions for the velocities were assigned from a circumpolar setup of MITgcm with 0.25° resolution that was run with identical atmospheric forcing (Holland et al., 2014). The model was spun-up for 10 years with atmospheric forcing from NCEP CFSR 1980 and then run from 1979 to 2011. The model does not include tides, however typical observed maximum tidal velocities range from 1 to 4 cm s^{-1}, less than typical average velocities at many locations (Wåhlin et al., 2012).

3.3 Iceberg detection

Studies of icebergs in the Southern Ocean have been carried out using a variety of methods, including ship based observations, (Jacka & Giles, 2007; Romanov et al., 2011), in-situ sensors on icebergs (Scambos et al., 2008), drift models (Gladstone et al., 2001) and satellite based systems, such as radar altimetry (Tournadre et al., 2008; Tournadre et al., 2016), microwave scatterometry (Stuart & Long, 2011), visual and near-infrared (VIR) sensors (Bindschadler, 2002) and synthetic aperture radar (SAR, Young et al., 1998; Wesche & Dierking, 2015, Mazur et al., 2017). Generally, the low resolution of the scatterometers makes this sensor type suitable for very large icebergs only and radar altimetry does not give reliable results in areas with high sea ice concentration. The dependency of cloud cover and light conditions of the VIR sensors is problematic in polar regions. Despite the computational demands and elaborate image processing, the ability of SAR systems to continuously acquire high resolution images in all atmospheric conditions make them suitable for remote sensing of high latitude areas with heavy sea ice cover.

In contrast to the passive altimeters and scatterometers, SAR is an active system, which carries its own source of radiation to illuminate the target (Rees, 2013). The sensor sends out a microwave pulse and measures the backscattered energy (Figure 12), which is dependent on the beam angle, radar beam penetration and roughness of the illuminated area. The distance traveled by the sensor over the target in the time taken for the pulses to return to the antenna generates the synthetic antenna aperture. The image resolution is proportional to the length of the aperture. The actual physical antenna is usually around 10 meters long.

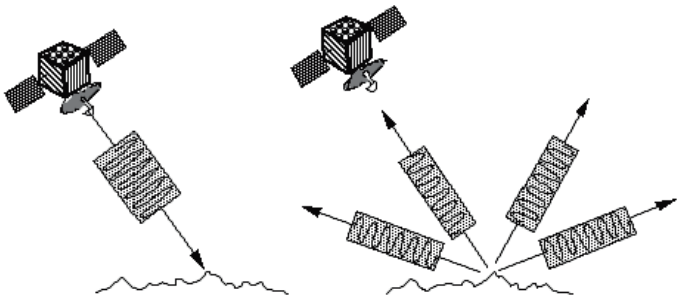

***Figure 12**. A radar antenna transmitting signals and receiving backscattered echoes. Credit: ESA.*

Envisat (Figure 13) is a satellite that was operated by the European Space Agency (ESA). It was launched on the 1st of March 2002 into a sun synchronous orbit circling the Earth in 101 minutes at an altitude of 790 km, with a repeat cycle of 35 days. The contact was lost with the satellite on 8th of April 2012, possibly due to power failure or short circuit (ESA declares end of mission for Envisat, 2012). It carried 10 Earth observation instruments including an ASAR sensor operated at C-band (5.3 GHz) and incidence angle 17°-43° (Envisat ASAR (Advanced SAR) Product Handbook, 2007).

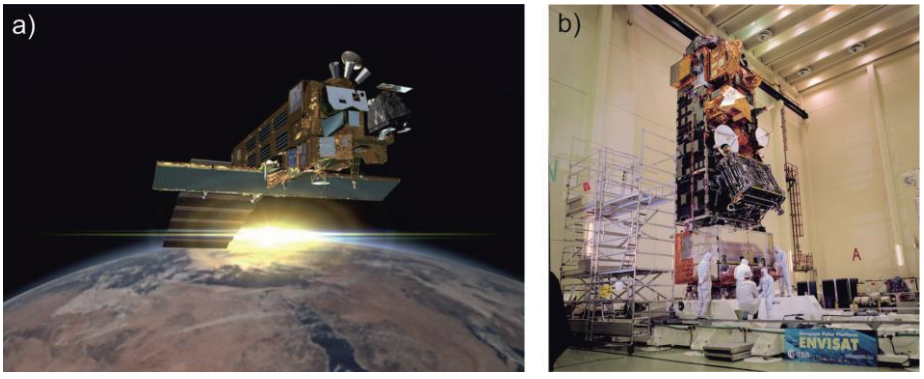

***Figure 13. a)** An artist´s impression of Envisat **b)** Envisat in the European Space Research and Technology Centre in Noordwijk, the Netherlands. Credit: ESA.*

The iceberg information used in paper V was based on ASAR data from Envisat. Icebergs were detected using an object-based algorithm developed by Mazur et al. (2017), applied on 2505 Wide Swath Mode Level 1 images recorded between Jan 2006 and Apr 2012. The images are first geo-located and radiometrically calibrated to the backscattering coefficient according to Rosich and Meadows (2004). Next the images are filtered using a Frost filer 3×3 to additionally remove speckle (Frost et al., 1982). In the following step, icebergs are identified using an object-oriented image interpretation with segmentation and classification carried out on different scale levels. Distinction of icebergs is then based on homogeneity, brightness, contrast and shape qualities with thresholds given on each scale. The icebergs which are distinguishable on different images are then manually tracked.

In the domain 70-75.5°S, 100-126°W (Figure 10), 56 non-stationary icebergs were identified, with areas ranging from 3 to 261 km^2 (average 20 km^2). The time step between iceberg observations, dependent on the average revisit frequency of the satellite, decreased from 9 days in 2006 to 2 days in 2012. Spatially, the best satellite coverage were in the southern and eastern areas close to the ice shelves, with around 40% coverage in the first years increasing to 50% the last two years (Aleksandra Mazur, pers. comm., 2016). The outer shelf area was less densely covered in the first two years, approximately 15 %, but increased to 50% in the last two years. The effect of low coverage resulted in longer time steps between observations and thus difficulties in tracking icebergs for their full path.

4 Contributions to understanding of the Amundsen Sea circulation

4.1 Continuous inflow of warm deep water (paper I)

The Amundsen Sea Embayment had started to attract research attention due to melting of the ice shelves, observed particularly at Pine Island Glacier. Warm deep water had been identified near Pine Island glacier by Jacobs et al. (1996) and in the entrance of the western Pine Island trough by Walker et al. (2007), but knowledge of temporal variations was still limited. In paper I, the structure and variability of the inflow of CDW in the Dotson-Getz trough, earlier observed by Wåhlin et al. (2010) using shipborne measurements, was investigated. Statistical methods were applied to the two year time series data from mooring S1. This was one of the earliest reports presenting in-situ ocean time series data from a "warm" Antarctic shelf, following the study by Arneborg et al. (2012)

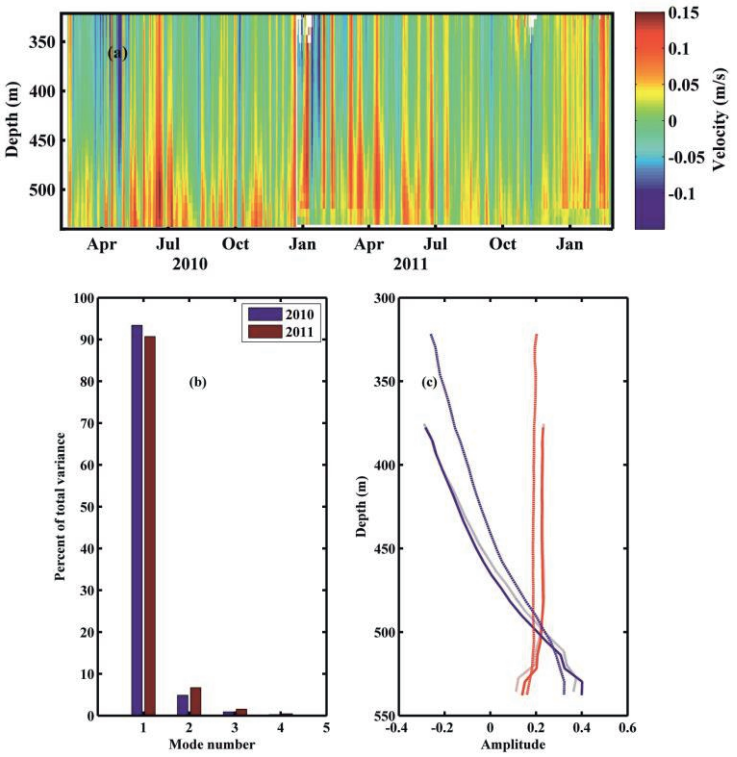

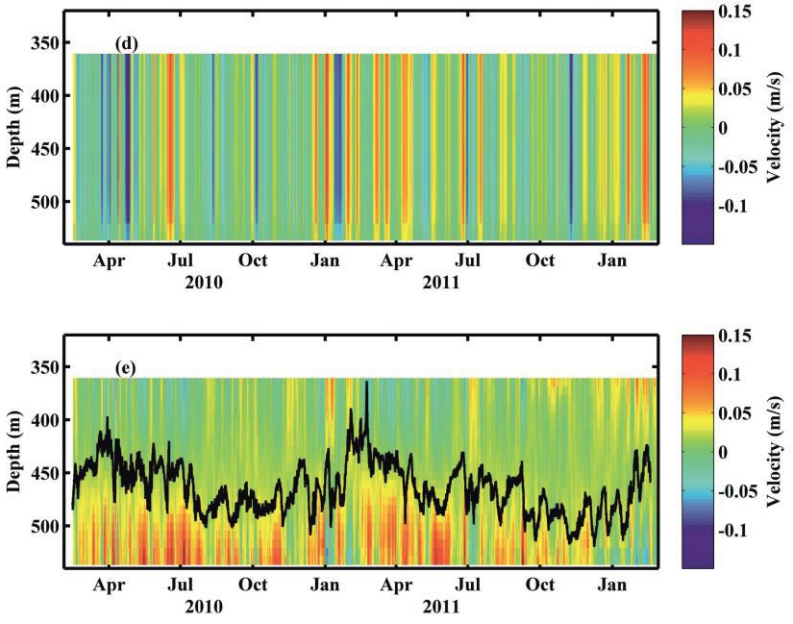

Figure 14. a) *Daily average of the along-trough velocity (positive values indicating southward flow) as a function of time and depth* ***b)*** *Percent of total variance that is explained by the first five EOF modes for the two years* ***c)*** *Shape of the first (red) and second (blue) EOF modes as a function of depth for 2010 (dashed), 2011 (dotted) and for the whole measurement period (solid)* ***d)*** *The first EOF mode for the whole measurement period* ***e)*** *Along-trough residue current, i.e. velocity minus the first EOF mode, with positive values indicating southward flow. Black line is the 0 ^{o}C isotherm.*

Warm deep water was found to be present in the bottom layer of the trough at all times. The black line in Figure 14e shows the 0°C isotherm, below which the temperature is above zero. The thickness of the warm water layer as well as maximum temperatures occurred during autumn (March-April-May). Thinner bottom layers containing cooler and fresher deep waters were found in spring (September-October-November) coinciding with maximum extent of the upper winter mixed layer.

The de-tided daily averaged velocity time series showed the dominance of energetic fluctuations on daily timescales with little vertical variability. The inflow component of the current, rotated to align with the channel isobaths, is shown in Figure 14a, has a vertical average of 2.4 cm s^{-1} for the whole time series. The cross-trough component is smaller, vertical average of -0.5 cm s^{-1} (towards SW), with less vertical variability. To investigate the structure of the

currents, we used empirical orthogonal functions (EOF) analysis, a method which finds patterns of variability, their temporal variation and rates the significance of each pattern (Björnsson & Venegas, 1997). The first EOF mode explains about 90% of the variance, 7% was contained in the second mode EOF (Figure 13b), leaving an insignificant contribution higher modes. The vertical structure of the mode shapes are given in Figure14c, where EOF1 shows a nearly depth independent pattern, while EOF2 changes direction with depth. Keeping in mind that EOF analysis is a statistical procedure without physical connection, the flow in the lower half of the water column was interpreted to consist of a dominant energetic barotropic component and a smaller bottom-intensified part, shown in the time series of Figures 14d and e.

The connection between the mooring data and the wind was examined using daily and monthly averages of ERA-Interim (Dee et al., 2011) winds. Significant correlations of 0.4 were found between the eastward pseudo-stress (the product of the wind speed and the wind vector) and both the along trough EOF1 and the heat transport induced by the EOF1. This result is in agreement with circulation theory where eastward winds drive an Ekman transport away from the coast which is the compensated by an on shelf southward flow in the bottom layer. No significant correlations were found on monthly scales; however this result is also influenced by the limited length of the dataset. A widely cited modeling study by Thoma et al. (2008) had found a warm layer maximum in spring (September-October-November) as well as a correlation between the warm-layer thickness and eastward winds. Results from paper I did not support these results. However, it should be noted that the study by Thoma et al. (2008) was more focused on Pine Island Bay and used another reanalysis product for the winds (US National Centers for Environmental Prediction, NCEP, Kalnay et al., 1996). The general finding that eastward winds may force CDW intrusions on the shelf hold for both studies, but paper I pointed towards the importance of the velocity rather than the temperature of the inflows.

4.2 Clockwise channel circulation (paper II)

The pathways of the circulation of warm deep water in the Dotson-Getz trough were inferred from four moorings deployed during 2011. Results based mostly on recordings from the lower part of the water column at the moorings S1 and S2 (in paper II denoted as M1 and M2) showed that there was a southeastward inflow in approximate geostrophic balance on the eastern side, as reported earlier by Arneborg et al. (2012) and in paper I. In

paper II it was shown that there is also an outflow on the western side. The clockwise circulation and ice shelf melting by the deep currents were deduced from the observed northwestward flow of colder water on the western side of the channel at mooring S2.

Assessments of the amount of heat the currents can bring to the ice shelves were made. The total heat flux Q_H (W) through a cross-channel transect is given by

$$Q_H = \int_{x_1}^{x_N} \int_{-D}^{-d} \rho C_p U \left(T - T_R\right) dz\, dx \qquad (1)$$

where x is the horizontal coordinate (m) from grid point x_1 to x_N, $-D$ is the bottom depth (m), $-d$ is the level (m) up to which the integration is performed (the surface or the reach of the ADCP), ρ (kg m^{-3}) is the in-situ density, C_p (J K^{-1} kg^{-1}) is the specific heat capacity, dependent on the local temperature, salinity and pressure, U (m s^{-1}) is the along-trough velocity, T (K) is the temperature and T_R (K) is a reference temperature to which the water eventually cools. Since the moorings measure at one point in space only, the horizontal coordinate was approximated with an effective inflow width, a ratio between the geostrophic heat flux and the heat flux per unit width. At the inflow side, the length 80 km was used, based on data from the cross-trough transects in 2008 (Wåhlin et al., 2010) and 2010 (Paper II). The corresponding value used for the western side was 40 km.

The current directions were visualized using progressive vector diagrams, constructed by time-integration of the mooring velocities and giving pseudo vectors of downstream displacement. Results are shown in Figure 15a, where the red lines from the lower ADCP bins at S1 (panel M1) reveal that warm water flows toward southeast following the channel bathymetry. The outflowing waters at S2 (panel M2), also steered by local bathymetry in the bottom layers, are colder. Time average properties were temperature 0.8°C and salinity 34.5 on the inflow side and -0.4°C and 34.2 for the outflow. The seemingly cold water on the western side is still warm, salty and dense compared with the overlying surface layer.

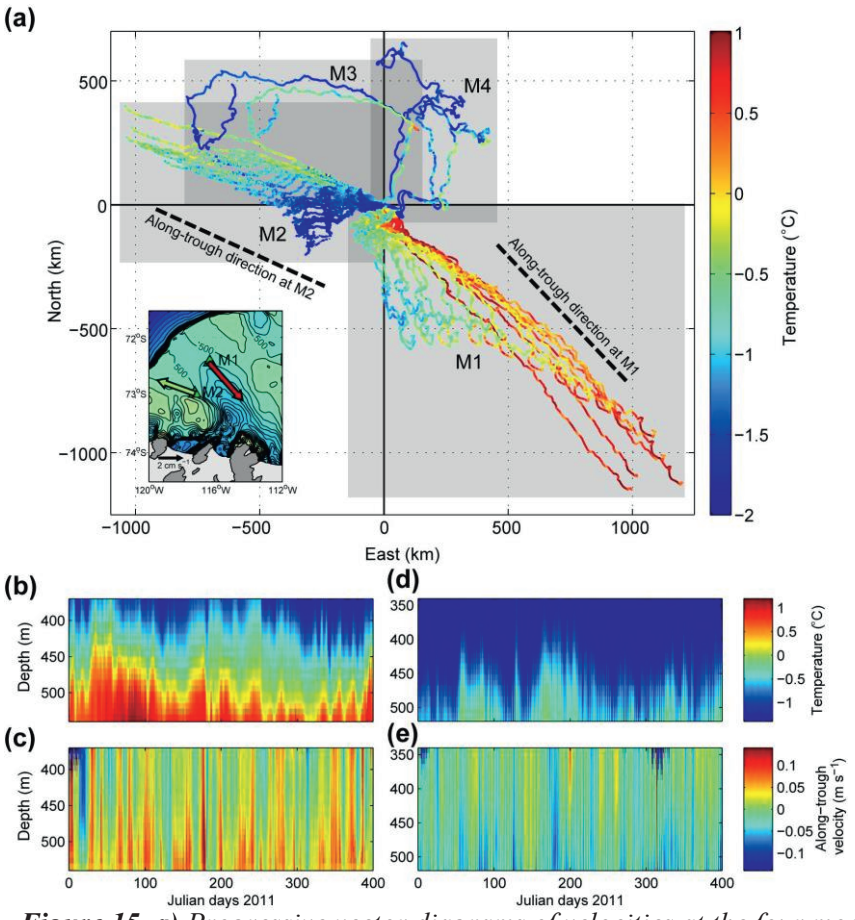

Figure 15. a) *Progressive vector diagrams of velocities at the four moorings, color coded by temperature. Data from M1and M2: the lines correspond to ADCP bins (every 8m) and interpolated temperature. Data from M3: the two lines correspond to the velocity and temperature at 409- and 253-m depth. Data from M4: the two lines correspond to the velocity and temperature at 431- and 276-m depth. Start time is 1000 UTC 1 Jan 2011. The ''along-trough direction'' at M1 andM2 is indicated by black dashed lines. Each gray rectangle encompasses the data from the designated mooring. The inset shows vectors of time-averaged currents (color coded by temperature) near the bottom at M1 and M2.(bottom) The 2-day low-pass-filtered mooring data as a function of time and depth for M1 and M2.* ***b)*** *Temperature and* ***c)*** *along-trough velocity at M1;* ***d)*** *temperature and* ***e)*** *along-trough velocity at M2. Along-trough velocities are calculated by the direction given in (a), and negative velocities indicate northwestward flow.*

Using the vertically integrated velocity time series and the effective transect widths, volume flows of deep water were estimated. Average inflow was 0.34 Sv (=10^6 m^3 s^{-1}) while the outflow was 0.12 Sv, thus only a third of the inflow exits as a cooled and freshened water mass at S2. The possible alternative routes for this water mass were hypothesized to be in the surface layers, in channels below the Getz ice shelf or in the western deep troughs, but further measurements are needed to solve this question. Using an assumption of long term conservation of volume and salt in the trough, computations of freshwater flux and corresponding latent heat to ice shelf melt were made. Of the different assessments, an intermediate weighted average freshwater flux taking the bottom inflow/outflow imbalance into account was deemed most realistic. The corresponding glacial melt was 237 Gt yr^{-1}. This value was seen to agree qualitatively with glaciological estimates using a satellite based input-output method by Rignot et al. (2013), who found melt rates of 145 Gt yr^{-1} for Getz ice shelf and 45 Gt yr^{-1} for Dotson ice shelf for the years 2007-2008.

4.3 Energetic current oscillations (paper III)

Energetic wavelike oscillations in the lower water column were discovered on the western outflow side of the Dotson-Getz trough. This phenomenon was detected through frequency domain analysis of the time series from mooring S2. The waves had power of similar magnitude to the oscillations caused by tides and Coriolis forces (due the rotation of the earth). Broad peaks in the power spectra around periods of 40-80 hours were also found for temperature, salinity, pressure and velocity, with a more pronounced signature in the cross-shelf direction. The time variability of the signal was examined using wavelet-analysis (Torrence & Compo, 1998) and it turned out that oscillations were present throughout the whole measurement period (2011-2013), with a handful of events causing more elevated energy levels. This signal was nonexistent in all data from mooring S1 on the eastern slope.

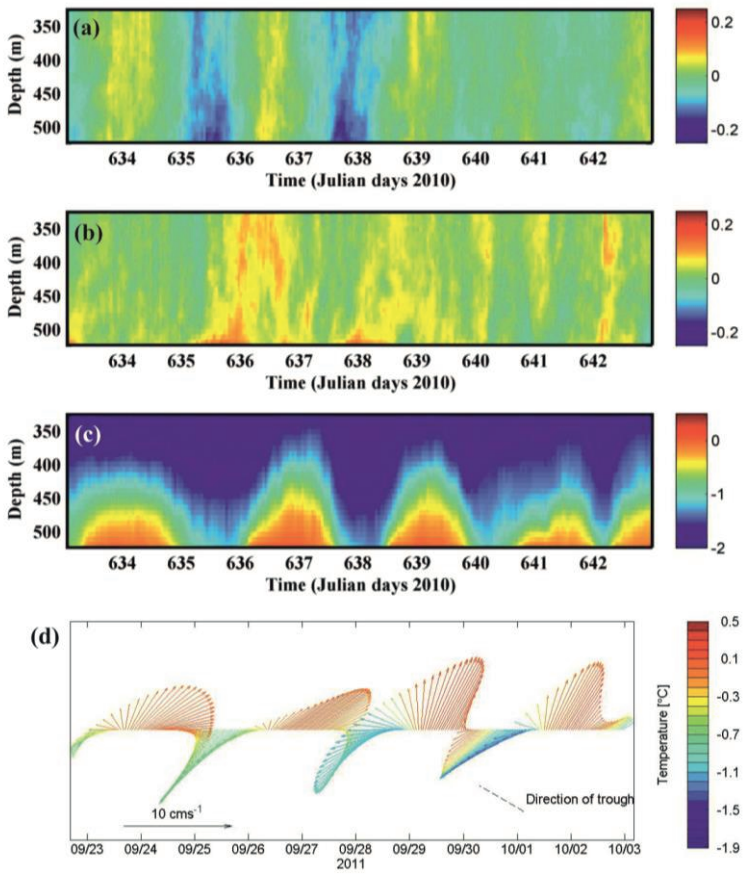

Figure 16. *Oscillations in velocity and temperature.* ***a)*** *Detided across-trough velocity component (ms^{-1})* ***b)*** *Detided along-trough velocity component.* ***c)*** *Temperature (°C).* ***d)*** *Quiver plot showing low-passed velocity anomalies from S2, 100 meters above bottom (mab). The velocity scale is given in the lower-left corner and the color of the arrow indicates the temperature at 100 mab. The dashed, black line indicates the direction of the trough. Dates are given in the format month/day.*

The powerful oscillations were qualitatively similar throughout the year. One example is shown in Figure 16, a detailed view of temperature and velocity during one occurrence starting in the end of September 2011. The temperature (Figure 16c) co-vary with the velocity (Figures 16a-b), with colder temperatures connected to cross-trough southwestward currents and warmer waters associated with northeastward flow, implying an up- and

downward movement of the bottom warm water layer on the side of the trough. The clockwise rotation of the current is evident in the vector plot (Figure 16d).

To characterize the wave oscillations, both a numerical code for computing topographically-trapped waves (Brink, 2006) with a measured multi-beam topography and an analytical solution from linear wave theory (Gill, 1982) with a simplified 1D topography were used. For the simplified geometry, the solution to the barotropic wave equation gives that for short waves, the energy (i.e. group speed) propagates with shallow water to the right, which is southeastward on the western trough slope. For long waves, the energy propagation is reversed. When wavelengths in both directions are approximately equal, they cancel each other out, the group speed approaches zero, which means that the energy does not move away and resonant waves are formed. The frequency at which topographic Rossby waves of the first mode had zero group velocity were close the observed values for the mooring spectra. These results agreed qualitatively for both the analytical and model solutions.

Resonant topographic Rossby waves can be forced by the wind, as shown by Gordon and Huthnance (1987) on the Scottish continental shelf and Miller et al. (1996) on the Iceland Faroe ridge. The high spectral coherence (0.69) between the cross-shelf velocity and the wind at S2 pointed towards the importance of wind forcing also in our area. Apart from the value of reporting for the first time about a novel wave phenomenon on the Antarctic continental shelf, the major implication from the results of Paper III is that sporadic hydrographic measurements in this area are of limited value. Single snapshot CTD and ADCP measurements will be severely biased if they should be taken during a major Rossby wave event.

4.4 Structure of the oceanic heat transport (paper IV)

This study expanded on the knowledge gained in paper I and II about the heat transport by inflowing deep warm currents and their clockwise circulation in the trough. Whereas the earlier studies derived conclusions using data from the lower part of the water column, the main research inquiry in paper IV was to investigate the full depth via the question of the vertical structure of the warm water circulation. To help cover for the lack of upper layer data from the moorings, the numerical ocean model (Assmann et al., 2013) described in section 3.3, two cross-shelf transects and a small selection of shipborne drift

station data were used. An additional goal was to assess the accuracy of the model simulations with comparisons to the observations.

In general, the model output showed good qualitative agreement with the observations, with a warm water bottom layer on the eastern trough slope and an outflowing colder current on the western side. The magnitudes of temperature were relatively similar, but the model produced a warm bottom layer that was thicker than in the observations. The smaller scale variability in the observations is lacking in the model, an indication that the resolution may be to coarse to resolve all physical processes (St-Laurent et al., 2015). Modeled and measured velocities were relatively similar, except for a lack of occasional periods on inflow on the western side in the model which were seen in the observations. The position of the inflow core was offset in the model due to the discrepancy between the model bathymetry (Timmermann et al., 2010) and the actual depths as measured with ship mounted multi-beam echo sounding. The center of the trough is in reality 150 m deeper and positioned 20 km further west compared with the model bathymetry, which highlights the importance of accurate bathymetry to increase model precision.

The barotropic velocity was defined as the vertical average of the current and the baroclinic velocity is then the remaining depth varying part of the current, both channel-rotated as in the previous papers. Just as the total flow was expressed as a sum of two parts, the total heat flux Q_H through a cross-channel transect (Equation 1) was also partitioned into a barotropic and a baroclinic flow component. The cross-channel transect was split in two parts at the deepest point of the trough to distinguish between the inflowing eastern side and the outflowing western slope of the channel.

Results from the heat flux calculations are shown in Figure 17, where the dominance of the barotropic part is evident both in the model and observational data. The time averaged heat fluxes (positive towards the continent) of 3.25 TW from the mooring data on eastern side and -0.70 TW on the western side are of similar magnitudes as those found in paper II. The average heat fluxes in the model have a smaller inflow of 2.10 TW, and a larger outflow of -1.63 TW. The discrepancies between the observations and model on the eastern side could be due to the shallow model bathymetry and on the western slope, the periods of inflowing velocities found in the observations are absent in the model.

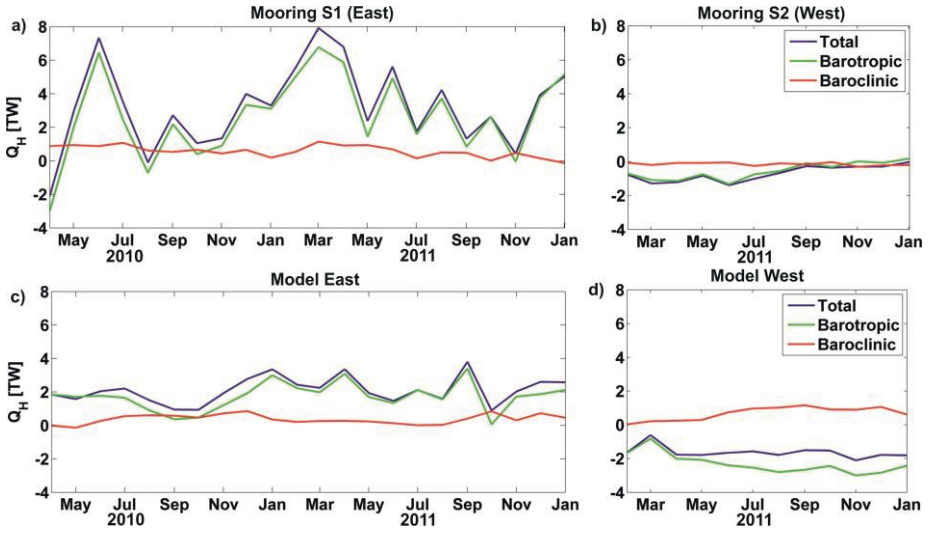

Figure 17*. Time series of monthly heat fluxes (TW) induced by the velocity components along the cross-trough sections. Times correspond to the deployment periods of the two moorings.* ***a)*** *Eastern part, observational data.* ***b)*** *Western part, observational data.* ***c)*** *Eastern part, model data.* ***d)*** *Western part, model data.*

Heat fluxes were also computed for the whole modeled time period 1980-2011, which showed some variability in the magnitude of fluxes, but with the same qualitative result as the shorter period above, which also had observational data. The finding that barotropic flow is responsible for the major part of the heat flux in the channel may thus be valid for a longer time frame.

Implications of the findings regarding the forcing of the heat flux can be drawn. Once the warm deep water has been delivered onto the shelf, its circulation in the shelf break trough occurs mainly as a clockwise barotropic flow. The depth-independent structure of the currents indicate that they may be forced by local winds, as opposed to earlier investigations (Arneborg et al., 2012; Wåhlin et al., 2012), suggesting the flow being buoyancy forced and thus more dependent on off-shelf drivers.

4.5 Upper ocean currents and iceberg drift (paper V)

Efforts on describing the ocean circulation on the Amundsen Sea continental shelf have so far mostly been focused on the lower part of the water column and on local channel patterns rather than a regional overview. The aim of paper V was to increase the knowledge about the general upper layer circulation. This was accomplished by combining in situ ocean measurements and ocean model output (same as in paper IV) with iceberg tracks and atmospheric forcing fields derived from satellite data. The icebergs were here treated as surface drifters and the drivers of the iceberg speed were investigated. The iceberg detection algorithm (Mazur et al., 2017) used in this study was described in section 3.3. Apart from their use in revealing ocean currents, icebergs are also an important source of freshwater and approximately half of the mass loss from all Antarctic glaciers is attributed to iceberg calving (Depoorter et al., 2013).

The force balance of horizontal iceberg motion is a sum of the Coriolis acceleration, air drag, water drag and sea ice drag (Gladstone et al., 2001). In open ocean free-drift, the dominant contributions come from the air and water drag and to a lesser degree the Coriolis forces. Large icebergs normally follow geostrophic currents in light wind conditions, but in winds exceeding 10 ms^{-1} their path get more deflected from the current (Crépon et al., 1988). The icebergs get locked into the sea ice when sea ice concentrations exceed 0.9 and their tracks are then controlled by the wind-induced sea ice drift (Lichey & Hellmer, 2001). The satellite data contained no information regarding the thickness of the icebergs, thus some assumptions of their draft had to be made to assess whether the lower part of the bergs did reach down to depths were the moored sensors measured the currents (approx. 200-400 m). The height of the major ice shelves from where the icebergs calved (Jacka & Giles, 2007; Liu et al., 2015) and the height to thickness ratios of icebergs (Orheim, 1980) hinted that many icebergs do reach down to the mooring depths. Furthermore, the observation of icebergs stranding on the 300 m deep ridge separating the Pine Island Trough from the Dotson-Getz Trough (Mazur et al., 2017) strengthened this assumption.

The icebergs were divided into four groups, according to origin and path taken (Figure 18). The overall conclusion is that there are two components of the upper layer drift. One part is a general shelf-wide drift towards west, as seen in all four groups of icebergs. The probable explanation to this pattern is that the ocean surface stress (Kim et al., 2017), forced by both wind and sea ice drift, produces a westward surface Ekman transport. The other part is

more local scale where currents are topographically steered by the bathymetry and move with shallow water to the left, as also found in model studies (Schodlok et al., 2012; St-Laurent et al., 2013) and in measurements of near-bottom currents in the Pine Island (Jacobs et al., 2011) and Dotson-Getz troughs (Paper II). This structure can be seen in paths of the icebergs circling into (Figure 18d) and out of (Figure 18b) Pine Island bay.

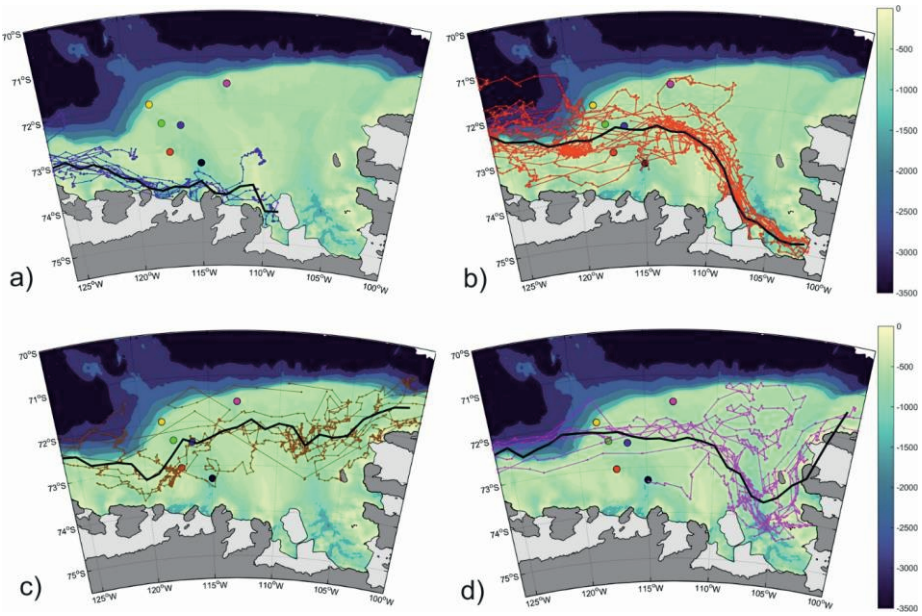

***Figure 18**. Iceberg tracks. Black lines show average latitude for every 1° longitude segment. **a)** Costal current group, 13 icebergs, average velocity 4 cms^{-1}. **b)** Pine Island group, 25 icebergs, avg. velocity 5 cms^{-1}. **c)** Bellingshausen/Abbot North group, 9 icebergs, which never go south of Burke Island, avg. velocity 6 cms^{-1}. **d)** Bellingshausen/Abbot South group, 9 icebergs, avg. velocity 7 cms^{-1}. Averages were calculated without speeds lower than 0.5 cms^{-1}.*

Of the six moorings used in this study (Table 1, Figure 10), current data from the four on shelf moorings, S1,S2, K1 and K2, also showed a general clockwise circulation. Within their substantial directional spread, they all also contained westward components indicating the shelf wide drift pattern. The moorings closer to the shelf break, BSR 12 and BSR 14 have deeper sensors

and their higher more unidirectional velocities may be influenced by undercurrents at the shelf break (Walker et al., 2013) and thus less connected to the upper layer circulation. The model circulation clearly showed the clockwise channel circulation and also the westward coastal current (Kim et al., 2016) influencing the drift of icebergs outside Getz and Dotson ice shelves (Figure 18a). The westward drift was however not very evident in the model data.

5 Conclusions and future outlook

The results from papers I-V were summarized in the previous chapter. The most important general conclusions in this thesis are:

- On the eastern slope of the Dotson-Getz trough there is always warm deep water present. There is large variability in the currents on daily and sub-daily timescales. Maximum temperatures and warm layer thickness occur during autumn (March-April-May). The inflow velocity is correlated with eastward winds over the shelf area.

- The inflowing warm deep waters melt the floating ice shelves and exit at the western side of the trough. Alternative paths for the cooled and freshened water mass on the western side exist. The assessed glacial melt rates from the in-situ data correspond roughly to satellite based estimates.

- Resonant topographic Rossby waves were identified on the western side of the Dotson-Getz trough. The oscillating wave motions, which are present almost all the time, are powerful and sometimes dominate current variability. Their presence makes conclusions drawn from snap-shot station data in this area less valuable.

- The Southern Ocean bathymetry databases have large errors on the Amundsen Sea shelf. The errors make results from modeling studies as well as flow and transport calculations less reliable.

- A depth independent barotropic flow appears to be the most important part of the current circulation on the shelf, which transport the heat in the trough.

- The regional upper layer ocean circulation on the Amundsen Sea continental shelf has two components. One is a general large scale drift towards west and the other is a more local clockwise circulation, steered by bathymetry in the glacial cross-shelf troughs.

This thesis research contributes to our knowledge of the rapid changes taking place around the Antarctic continent, which is the earth´s largest source of freshwater. The heat supplying deep ocean currents have been investigated using in-situ measurements, ocean modeling and remote sensing. The shorter term variability with its drivers are now better understood, but one of the aspects that are lacking is more decisive analyses of seasonal variation, which have so far been discouraged by the lack of adequately long time series. The S1 mooring currently contains six years of unbroken measurements and is hopefully still functional. The possibly longest time series from a warming Antarctic shelf may now be used to shed some light on seasonal variability. This data could also be used to investigate the ocean dependency on climate indices, such as El Niño-Southern Oscillation, the Southern Annular Mode and the variability of the Amundsen Sea Low, which have a significant influence in the area (Jenkins et al., 2016).

Another exciting future project is the analysis of data from new moorings currently employed in the western part of Getz Ice Shelf at approximately 128°W. There exists no ocean time series data from this part of the vast Getz Ice Shelf, a severe limitation to the knowledge of the future development of Antarctic ice shelves. The Getz area also acts as a connection between a hypothesized westward drift of warm deep waters from around the West Antarctic Peninsula (Bromwich et al., 2012) and Bellingshausen Seas (Holland et al., 2010) towards the colder Ross Sea (Jacobs & Guilivi, 1998; Comiso et al., 2011) where large amounts of sea ice and dense High Salinity Shelf Water is produced.

One of the most pressing priorities for Antarctic research is to increase measurement frequency in the under-sampled Southern Ocean, both in space and time (Kennicut et al., 2014; Schofield et al., 2016). It is also necessary with more measurements from the ice-ocean interface below the floating ice shelves (Jenkins et al., 2012) in order to better understand the complex interactions and improve modeling efforts. The melting may be highly influenced by the geometry of gigantic sub ice shelf cavities (Dutrieux et al., 2014) whose extent and shape remain basically unknown. These formerly impossible ocean observations (Nicholls et al., 2008) can now be realized with the aid of an Autonomous Underwater Vehicle (AUV), a mini-submarine equipped with high-resolution sensors, deployed from an icebreaker to then go on a mission under the ice shelves. The Polar Oceanography group at University of Gothenburg have been leading the formation of the national infrastructure facility for marine research called MUST (Mobile Underwater System Tools), which will include an under-ice going AUV. The planned deployment of the AUV under the Getz Ice Shelf

will be an important step towards a better understanding of what has been termed the greatest remaining unsolved problem when predicting future global sea level rise (Stocker et al., 2013; Kennicut et al., 2014), the fate of the West Antarctic Ice Sheet.

Acknowledgements

First I would like to express my sincere gratitude to the most important person in this project, my supervisor Anna Wåhlin. I would not have come as far down the road to higher knowledge without your unwavering enthusiasm and never ending energy. Feelings of despair and gloom have been kept at bay by your ability to turn setbacks into possibilities. I have come to see the merits of a general outlook where expectation of success rather than fear of failure is the guiding assumption. Thank you for your trust in my abilities to pull this thing off and taking me on this journey. Also thanks to my assistant supervisor Leif Eriksson for making this project happen.

My fellow PhD students at the Marine Science and Earth Science departments deserve many thanks for their support and sharing of ideas, especially my former and present roommates Sam Fredriksson and Aleksandra Mazur as well as Ardo Robijn. We have shared the sometimes strange predicament of trying to learn how to move forward in the world of science. Thank you for all your help, understanding and encouragement and good luck in your futures.

Numerous colleagues, co-workers and collaborators have been instrumental in my progress and I am indebted to many who are not mentioned in this short text. Before I started this thesis work, I had the great fortune to work together with Anders Stigebrandt, the ultimate out-of-the-box thinker who will hopefully be able to save the Baltic Sea. Many thanks to Lars Arneborg, my supportive and insightful supervisor during two degree projects on the exciting theme of wave energy extraction. Thank you Karen Assmann, for sharing valuable output and deep knowledge from the world of ocean modelling. Göran Björk is thanked for collaborative work on papers and also for ensuring the quality of my work in his role as examiner. One part of my employment has been dedicated to teaching, thanks to all engaged and curious marine science students, you are our hope for the future. The courses were led by Torsten Linders, whose devotion to ocean science teaching has been inspiring. Furthermore, thanks Clara Calander for good company on expeditions.

To all my friends and family, thanks for all your patience and support. To Arve, Tore and Stina – eternal love.

References

Antonov, J. I., Seidov, D., Boyer, T. P., Locarnini, R. A., Mishonov, A. V., Garcia, H. E., . . . Johnson, D. R. (2010). World Ocean Atlas 2009. *S. Levitus Ed. NOAA Atlas NESDIS 69, Volume 2: Salinity*.

Arndt, J. E., Schenke, H. W., Jakobsson, M., Nitsche, F. O., Buys, G., Goleby, B., . . . Wigley, R. (2013). The International Bathymetric Chart of the Southern Ocean (IBCSO) Version 1.0-A new bathymetric compilation covering circum-Antarctic waters. *Geophysical Research Letters, 40*(12), 3111-3117. doi:10.1002/grl.50413

Arneborg, L., Wåhlin, A. K., Björk, G., Liljebladh, B., & Orsi, A. H. (2012). Persistent inflow of warm water onto the central Amundsen shelf. *Nature Geoscience, 5*(12), 876-880. doi:10.1038/ngeo1644

Assmann, K. M., Jenkins, A., Shoosmith, D. R., Walker, D. P., Jacobs, S. S., & Nicholls, K. W. (2013). Variability of Circumpolar Deep Water transport onto the Amundsen Sea Continental shelf through a shelf break trough. *Journal of Geophysical Research: Oceans, 118*(12), 6603-6620. doi:10.1002/2013jc008871

Biddle, L. C., Kaiser, J., Heywood, K. J., Thompson, A. F., & Jenkins, A. (2015). Ocean glider observations of iceberg-enhanced biological production in the northwestern Weddell Sea. *Geophysical Research Letters, 42*(2), 459-465. doi:10.1002/2014gl062850

Bindschadler, R. A. (2002). History of lower Pine Island Glacier, West Antarctica, from Landsat imagery. *Journal of Glaciology, 48*(163), 536-544.

Bintanja, R., Van Oldenborgh, G. J., & Katsman, C. A. (2015). The effect of increased fresh water from Antarctic ice shelves on future trends in Antarctic sea ice. *Annals of Glaciology, 56*(69), 120-126. doi:10.3189/2015AoG69A001

Björk, G., Söderkvist, J., Winsor, P., Nikolopoulos, A., & Steele, M. (2002). Return of the cold halocline layer to the Amundsen Basin of the Arctic Ocean: Implications for the sea ice mass balance. *Geophysical Research Letters, 29*(11). doi:10.1029/2001gl014157

Björnsson, H., & Venegas, S. A. (1997). A manual for EOF and SVD analyses of climatic data. *CCGCR Report, 97*(1), 112-134.

Brink, K. H. (2006). Coastal-trapped waves with finite bottom friction. *Dynamics of Atmospheres and Oceans, 41*(3-4), 172-190. doi:10.1016/j.dynatmoce.2006.05.001

Bromwich, D. H., Nicolas, J. P., Monaghan, A. J., Lazzara, M. A., Keller, L. M., Weidner, G. A., & Wilson, A. B. (2012). Central West Antarctica among the most rapidly warming regions on Earth. *Nature Geoscience, 6*(2), 139-145. doi:10.1038/ngeo1671

Bumbaco, K. A., Hakim, G. J., Mauger, G. S., Hryniw, N., & Steig, E. J. (2014). Evaluating the Antarctic Observational Network with the Antarctic Mesoscale Prediction System (AMPS). *Monthly Weather Review, 142*(10), 3847-3859. doi:10.1175/mwr-d-13-00401.1

Cavalieri, D. J., Parkinson, C. L., Gloersen, P., & Zwally, H. (1996). Sea Ice Concentrations from Nimbus-7 SMMR and DMSP SSM/I-SSMIS Passive Microwave Data. *NASA DAAC at the Natl. Snow and Ice Data Cent., Boulder, Colorado. (Updated yearly).*

Clark, P. U., Dyke, A. S., Shakun, J. D., Carlson, A. E., Clark, J., Wohlfarth, B., . . . Marshall McCabe, A. (2009). The Last Glacial Maximum. *Science, 325*(5941), 710-714.

Comiso, J. C., Kwok, R., Martin, S., & Gordon, A. L. (2011). Variability and trends in sea ice extent and ice production in the Ross Sea. *Journal of Geophysical Research, 116*(C4). doi:10.1029/2010jc006391

Connolley, W. M. (1997). Variability in annual mean circulation in southern high latitudes. *Climate Dynamics, 13*(10), 745-756.

Crépon, M., Houssais, M. N., & Guily, B. S. (1988). The drift of icebergs under wind action. *Journal of Geophysical Research, 93*(C4), 3608. doi:10.1029/JC093iC04p03608

Day, D. (2013). Antarctica: a biography. *Oxford University Press*.

Dee, D. P., Uppala, S. M., Simmons, A. J., Berrisford, P., Poli, P., Kobayashi, S., . . . Vitart, F. (2011). The ERA-Interim reanalysis: configuration and performance of the data assimilation system. *Quarterly Journal of the Royal Meteorological Society, 137*(656), 553-597. doi:10.1002/qj.828

Depoorter, M. A., Bamber, J. L., Griggs, J. A., Lenaerts, J. T., Ligtenberg, S. R., van den Broeke, M. R., & Moholdt, G. (2013). Calving fluxes and basal melt rates of Antarctic ice shelves. *Nature, 502*(7469), 89-92. doi:10.1038/nature12567

Ding, Q., Steig, E. J., Battisti, D. S., & Küttel, M. (2011). Winter warming in West Antarctica caused by central tropical Pacific warming. *Nature Geoscience, 4*(6), 398-403. doi:10.1038/ngeo1129

Dinniman, M., Asay-Davis, X., Galton-Fenzi, B., Holland, P., Jenkins, A., & Timmermann, R. (2016). Modeling Ice Shelf/Ocean Interaction in Antarctica: A Review. *Oceanography, 29*(4), 144-153. doi:10.5670/oceanog.2016.106

Doake, C. S. M., Corr, H. F. J., Rott, H., Skvarca, P., & Young, N. W. (1998). Breakup and conditions for stability of the northern Larsen Ice Shelf, Antarctica. *Nature, 391*(6669), 778-780.

Dutrieux, P., Stewart, C., Jenkins, A., Nicholls, K. W., Corr, H. F. J., Rignot, E., & Steffen, K. (2014). Basal terraces on melting ice shelves. *Geophysical Research Letters, 41*(15), 5506-5513. doi:10.1002/2014gl060618

Envisat ASAR Product Handbook. (2007). Issue 2.2. Retrieved from https://earth.esa.int/pub/ESA_DOC/ENVISAT/ASAR/asar.ProductHandbook.2_2.pdf

ESA declares end of mission for Envisat. (2012). Retrieved from http://www.esa.int/Our_Activities/Observing_the_Earth/Envisat/ESA_declares_end_of_mission_for_Envisat March 21, 2017

Fowler, C., Emery, W., & Tschudi, M. (2013). Polar Pathfinder Daily 25 km EASE-Grid Sea Ice Motion Vectors. Version 2. 2010-2011. *NASA DAAC at the National Snow and Ice Data Center, Boulder, Colorado USA*.

Fretwell, P., Pritchard, H. D., Vaughan, D. G., Bamber, J. L., Barrand, N. E., Bell, R., . . . Zirizzotti, A. (2013). Bedmap2: improved ice bed, surface and thickness datasets for Antarctica. *The Cryosphere, 7*(1), 375-393. doi:10.5194/tc-7-375-2013

Frost, V. S., Stiles, J. A., Shanmugan, K. S., & Holtzman, J. C. (1982). A model for radar images and its application to adaptive digital filtering of multiplicative noise. *IEEE Transactions on pattern analysis and machine intelligence, 2*, 157-166.

Gill, A. E. (1982). Atmosphere-ocean dynamics. *Elsevier*.

Gille, S. T. (2008). Decadal-Scale Temperature Trends in the Southern Hemisphere Ocean. *Journal of Climate, 21*(18), 4749-4765. doi:10.1175/2008jcli2131.1

Gladstone, R. M., Bigg, G. R., & Nicholls, K. W. (2001). Iceberg trajectory modeling and meltwater injection in the Southern Ocean. *Journal of Geophysical Research: Oceans, 106*(C9), 19903-19915. doi:10.1029/2000jc000347

Gordon, R. L., & Huthnance, J. M. (1987). Storm-driven continental shelf waves over the Scottish continental shelf. *Continental Shelf Research, 7*(9), 1015-1048.

Hastings, D. A., Dunbar, P. K., Elphingstone, G. M., Bootz, M., Murakami, H., Maruyama, H., ... , & Logan, T. L. (1999). The global land one-kilometer base elevation (GLOBE) digital elevation model, version 1.0. National Oceanic and Atmospheric Administration. *National Geophysical Data Center*(325, 80305-3328).

Hattermann, T., Nøst, O. A., Lilly, J. M., & Smedsrud, L. H. (2012). Two years of oceanic observations below the Fimbul Ice Shelf, Antarctica. *Geophysical Research Letters, 39*(12), n/a-n/a. doi:10.1029/2012gl051012

Heywood, K., Biddle, L., Boehme, L., Dutrieux, P., Fedak, M., Jenkins, A., . . . Webber, B. (2016). Between the Devil and the Deep Blue Sea: The Role of the Amundsen Sea Continental Shelf in Exchanges Between Ocean and Ice Shelves. *Oceanography, 29*(4), 118-129. doi:10.5670/oceanog.2016.104

Holland, P. R., Bruneau, N., Enright, C., Losch, M., Kurtz, N. T., & Kwok, R. (2014). Modeled Trends in Antarctic Sea Ice Thickness. *Journal of Climate, 27*(10), 3784-3801. doi:10.1175/jcli-d-13-00301.1

Holland, P. R., Jenkins, A., & Holland, D. M. (2010). Ice and ocean processes in the Bellingshausen Sea, Antarctica. *Journal of Geophysical Research, 115*(C5). doi:10.1029/2008jc005219

Hosking, J. S., Orr, A., Bracegirdle, T. J., & Turner, J. (2016). Future circulation changes off West Antarctica: Sensitivity of the Amundsen Sea Low to projected anthropogenic forcing. *Geophysical Research Letters, 43*(1), 367-376. doi:10.1002/2015gl067143

Jacka, T. H., & Giles, A. B. (2007). Antarctic iceberg distribution and dissolution from ship-based observations. *Journal of Glaciology, 53*(182), 341-356.

Jacobs, S. S., & Giulivi, C. F. (1998). Interannual ocean and sea ice variability in the Ross Sea. *Ocean, Ice, and Atmosphere: Interactions at the Antarctic Continental Margin (eds S. S. Jacobs and R. F. Weiss)*, American Geophysical Union, Washington, D. C.135-150.

Jacobs, S. S., Hellmer, H. H., & Jenkins, A. (1996). Antarctic Ice Sheet melting in the southeast Pacific. *Geophysical Research Letters, 23*(9), 957-960. doi:10.1029/96gl00723

Jacobs, S. S., Helmer, H. H., Doake, C. S. M., Jenkins, A., & Frolich, R. M. (1992). Melting of ice shelves and the mass balance of Antarctica. *Journal of Glaciology, 38*(130), 375-387.

Jacobs, S. S., Jenkins, A., Giulivi, C. F., & Dutrieux, P. (2011). Stronger ocean circulation and increased melting under Pine Island Glacier ice shelf. *Nature Geoscience, 4*(8), 519-523. doi:10.1038/ngeo1188

Jenkins, A., Dutrieux, P., Jacobs, S., McPhail, S., Perrett, J., Webb, A., & White, D. (2012). Autonomous Underwater Vehicle Exploration of the Ocean Cavity Beneath an Antarctic Ice Shelf. *Oceanography, 25*(3), 202-203. doi:10.5670/oceanog.2012.95

Jenkins, A., Dutrieux, P., Jacobs, S., Steig, E., Gudmundsson, H., Smith, J., & Heywood, K. (2016). Decadal Ocean Forcing and Antarctic Ice Sheet Response: Lessons from the Amundsen Sea. *Oceanography, 29*(4), 106-117. doi:10.5670/oceanog.2016.103

Jenkins, A., Dutrieux, P., Jacobs, S. S., McPhail, S. D., Perrett, J. R., Webb, A. T., & White, D. (2010). Observations beneath Pine Island Glacier in West Antarctica and implications for its retreat. *Nature Geoscience, 3*(7), 468-472. doi:10.1038/ngeo890

Joughin, I., Smith, B. E., & Medley, B. (2014). Marine ice sheet collapse potentially under way for the Thwaites Glacier Basin, West Antarctica. *Science, 344*(6185), 735-738.

Kalnay, E., Kanamitsu, M., Kistler, R., Collins, W., Deaven, D., Gandin, L., & ... & Zhu, Y. (1996). The NCEP/NCAR 40-year reanalysis project. *Bulletin of the American Meteorological Society, 77*(3), 437-471.

Kawaguchi, S., Ishida, A., King, R., Raymond, B., Waller, N., Constable, A., . . . Ishimatsu, A. (2013). Risk maps for Antarctic krill under projected Southern Ocean acidification. *Nature Climate Change, 3*(9), 843-847. doi:10.1038/nclimate1937

Kennicutt, M. C., Chown, S. L., Cassano, J. J., Liggett, D., Massom, R., Peck, L. S., . . . Sutherland, W. J. (2014). Six priorities for Antarctic science. *Nature, 512*(7512), 23-25.

Kim, C.-S., Kim, T.-W., Cho, K.-H., Ha, H. K., Lee, S., Kim, H.-C., & Lee, J.-H. (2016). Variability of the Antarctic Coastal Current in the Amundsen Sea. *Estuarine, Coastal and Shelf Science, 181*, 123-133. doi:10.1016/j.ecss.2016.08.004

Kim, T. W., Ha, H. K., Wåhlin, A. K., Lee, S. H., Kim, C. S., Lee, J. H., & Cho, Y. K. (2017). Is Ekman pumping responsible for the seasonal variation of warm circumpolar deep water in the Amundsen Sea? *Continental Shelf Research, 132*, 38-48. doi:10.1016/j.csr.2016.09.005

Larter, R. D., Anderson, J. B., Graham, A. G. C., Gohl, K., Hillenbrand, C.-D., Jakobsson, M., . . . Spiegel, C. (2014). Reconstruction of changes in the Amundsen Sea and Bellingshausen Sea sector of the West Antarctic Ice Sheet since the Last Glacial Maximum. *Quaternary Science Reviews, 100*, 55-86. doi:10.1016/j.quascirev.2013.10.016

Lewis, E. L., & Perkin, R. G. (1981). The Practical Salinity Scale 1978: conversion of existing data. *Deep Sea Research Part A. Oceanographic Research Papers, 28*(4), 307-328.

Levitus, S., Antonov, J. I., Boyer, T. P., Baranova, O. K., Garcia, H. E., Locarnini, R. A., . . . Zweng, M. M. (2012). World ocean heat content and thermosteric sea level change (0-2000 m), 1955-2010. *Geophysical Research Letters, 39*(10), n/a-n/a. doi:10.1029/2012gl051106

Lichey, C., & Hellmer, H. (2001). Modeling Giant Iceberg Drift Under the Inuence of Sea Ice in the Weddell Sea. *Journal of Glaciology, 47*(158), 452-460(459).

Liu, Y., Moore, J. C., Cheng, X., Gladstone, R. M., Bassis, J. N., Liu, H., . . . Hui, F. (2015). Ocean-driven thinning enhances iceberg calving and retreat of Antarctic ice shelves. *Proc Natl Acad Sci U S A, 112*(11), 3263-3268. doi:10.1073/pnas.1415137112

Locarnini, R. A., Mishonov, A. V., Antonov, J. I., Boyer, T. P., Garcia, H. E., Baranova, O. K., . . . Johnson, D. R. (2010). World Ocean Atlas 2009. *S. Levitus, Ed., NOAA Atlas NESDIS 68, Volume 1: Temperature*.

Losch, M. (2008). Modeling ice shelf cavities in azcoordinate ocean general circulation model. *Journal of Geophysical Research, 113*(C8). doi:10.1029/2007jc004368

Losch, M., Menemenlis, D., Campin, J. M., Heimbach, P., & Hill, C. (2010). On the formulation of sea-ice models. Part 1: Effects of different

solver implementations and parameterizations. *Ocean Modelling, 33*(1-2), 129-144. doi:10.1016/j.ocemod.2009.12.008

Mankoff, K. D., Jacobs, S. S., Tulaczyk, S. M., & Stammerjohn, S. E. (2012). The role of Pine Island Glacier ice shelf basal channels in deep-water upwelling, polynyas and ocean circulation in Pine Island Bay, Antarctica. *Annals of Glaciology, 53*(60), 123-128. doi:10.3189/2012AoG60A062

Marshall, G. J. (2003). Trends in the Southern Annular Mode from Observations and Reanalyses. *Journal of Climate, 16*(24), 4134-4143.

Marshall, J., Adcroft, A., Hill, C., Perelman, L., & Heisey, C. (1997). A finite-volume, incompressible Navier Stokes model for studies of the ocean on parallel computers. *Journal of Geophysical Research, 102*(C3), 5753. doi:10.1029/96jc02775

Marshall, J., & Speer, K. (2012). Closure of the meridional overturning circulation through Southern Ocean upwelling. *Nature Geoscience, 5*(3), 171-180. doi:10.1038/ngeo1391

Mazur, A. K., Wåhlin, A. K., & Krężel, A. (2017). An object-based SAR image iceberg detection algorithm applied to the Amundsen Sea. *Remote Sensing of Environment, 189*, 67-83. doi:10.1016/j.rse.2016.11.013

McNeil, B. I., & Matear, R. J. (2008). Southern Ocean acidification: a tipping point at 450-ppm atmospheric CO2. *Proc Natl Acad Sci U S A, 105*(48), 18860-18864. doi:10.1073/pnas.0806318105

Meredith, M. P., Naveira Garabato, A. C., Hogg, A. M., & Farneti, R. (2012). Sensitivity of the Overturning Circulation in the Southern Ocean to Decadal Changes in Wind Forcing. *Journal of Climate, 25*(1), 99-110. doi:10.1175/2011jcli4204.1

Miller, A. J., Lermusiaux, P. F., & Poulain, P. M. (1996). A topographic–Rossby mode resonance over the Iceland–Faeroe Ridge. *Journal of Physical Oceanography, 26*(12), 2735-2747.

Mouginot, J., Rignot, E., & Scheuchl, B. (2014). Sustained increase in ice discharge from the Amundsen Sea Embayment, West Antarctica, from 1973 to 2013. *Geophysical Research Letters, 41*(5), 1576-1584. doi:10.1002/2013gl059069

Mueller, R. D., Padman, L., Dinniman, M. S., Erofeeva, S. Y., Fricker, H. A., & King, M. A. (2012). Impact of tide-topography interactions on basal melting of Larsen C Ice Shelf, Antarctica. *Journal of Geophysical Research: Oceans, 117*(C5), n/a-n/a. doi:10.1029/2011jc007263

Nakayama, Y., Timmermann, R., Schröder, M., & Hellmer, H. H. (2014). On the difficulty of modeling Circumpolar Deep Water intrusions onto the Amundsen Sea continental shelf. *Ocean Modelling, 84*, 26-34. doi:10.1016/j.ocemod.2014.09.007

Nicholls, K. W., Abrahamsen, E. P., Heywood, K. J., & Stansfield, K. (2008). High-latitude oceanography using the Autosub autonomous underwater vehicle. *Limnology and Oceanography: Methods, 53*(5), 2309-2320.

Nicolas, J. P., & Bromwich, D. H. (2011). Climate of West Antarctica and Influence of Marine Air Intrusions. *Journal of Climate, 24*(1), 49-67. doi:10.1175/2010jcli3522.1

Orheim, O. (1980). Physical characteristics and life expectance of tabular Antarctic icebergs. *Annals of Glaciology, 1*(1), 11-18.

Orsi, A. H., & Whitworth, T., III. (2005). Hydrographic Atlas of the World Ocean Circulation Experiment (WOCE). Volume 1: Southern Ocean (eds. M. Sparrow, P. Chapman and J. Gould). *International WOCE Project Office, Southampton, U.K.*

Padman, L., Fricker, H. A., Coleman, R., Howard, S., & Erofeeva, L. (2002). A new tide model for the Antarctic ice shelves and seas. *Annals of Glaciology, 34*(1), 247-254.

Paolo, F. S., Fricker, H. A., & Padman, L. (2015). Volume loss from Antarctic ice shelves is accelerating. *Science, 348*(6232), 327-331.

Pawlowicz, P., Beardsley, B., & Lentz, S. (2002). Classic tidal harmonic analysis including error estimates in MATLAB using T_TIDE. *Computers & Geosciences* 28.8 (2002): 929-937.

Pritchard, H. D., Ligtenberg, S. R., Fricker, H. A., Vaughan, D. G., van den Broeke, M. R., & Padman, L. (2012). Antarctic ice-sheet loss driven by basal melting of ice shelves. *Nature, 484*(7395), 502-505. doi:10.1038/nature10968

Randall-Goodwin, E., Meredith, M. P., Jenkins, A., Yager, P. L., Sherrell, R. M., Abrahamsen, E. P., . . . Stammerjohn, S. E. (2015). Freshwater distributions and water mass structure in the Amundsen Sea Polynya region, Antarctica. *Elementa: Science of the Anthropocene, 3*, 000065. doi:10.12952/journal.elementa.000065

Rees, W. G. (2013). Physical principles of remote sensing. *Cambridge University Press*.

Rignot, E., Jacobs, S., Mouginot, J., & Scheuchl, B. (2013). Ice Shelf Melting Around Antarctica. *Science, 341*(6143), 266-270.

Rignot, E., Mouginot, J., Morlighem, M., Seroussi, H., & Scheuchl, B. (2014). Widespread, rapid grounding line retreat of Pine Island, Thwaites, Smith, and Kohler glaciers, West Antarctica, from 1992 to 2011. *Geophysical Research Letters, 41*(10), 3502-3509. doi:10.1002/2014gl060140

Rintoul, S., Hughes, C., & Olbers, D. (2001). The Antarctic circumpolar current system. *In: Ocean Circulation and Climate/eds. G. Siedler, J. Church and J. Gould*, New York: Academic Press,271-302.

Robertson, R. (2013). Tidally induced increases in melting of Amundsen Sea ice shelves. *Journal of Geophysical Research: Oceans, 118*(6), 3138-3145. doi:10.1002/jgrc.20236

Romanov, Y. A., Romanova, N. A., & Romanov, P. (2011). Shape and size of Antarctic icebergs derived from ship observation data. *Antarctic Science, 24*(01), 77-87. doi:10.1017/s0954102011000538

Rosich, B., & Meadows, P. (2004). Absolute calibration of ASAR level 1 products generated with PF-ASAR. *ESA Document, Frascati, Italy*.

Saha, S., Moorthi, S., Pan, H.-L., Wu, X., Wang, J., Nadiga, S., . . . Goldberg, M. (2010). The NCEP Climate Forecast System Reanalysis. *Bulletin of the American Meteorological Society, 91*(8), 1015-1057. doi:10.1175/2010bams3001.1

Sallée, J.-B., Matear, R. J., Rintoul, S. R., & Lenton, A. (2012). Localized subduction of anthropogenic carbon dioxide in the Southern Hemisphere oceans. *Nature Geoscience, 5*(8), 579-584. doi:10.1038/ngeo1523

Scambos, T., Ross, R., Bauer, R., Yermolin, Y., Skvarca, P., Long, D., . . . Haran, T. (2008). Calving and ice-shelf break-up processes investigated by proxy: Antarctic tabular iceberg evolution during northward drift. *Journal of Glaciology, 54*(187), 579-591.

Scambos, T. A., Bell, R. E., Alley, R. B., Anandakrishnan, S., Bromwich, D. H., Brunt, K., . . . Yager, P. L. (2017). How much, how fast?: A science review and outlook for research on the instability of Antarctica's Thwaites Glacier in the 21st century. *Global and Planetary Change, 153*, 16-34. doi:10.1016/j.gloplacha.2017.04.008

Schmidtko, S., Heywood, K. J., Thompson, A. F.,, & Aoki, S. (2014). Multidecadal warming of Antarctic waters. *Science, 346*(6214), 1227-1231.

Schodlok, M. P., Menemenlis, D., Rignot, E., & Studinger, M. (2012). Sensitivity of the ice-shelf/ocean system to the sub-ice-shelf cavity shape measured by NASA IceBridge in Pine Island Glacier, West Antarctica. *Annals of Glaciology, 53*(60), 156-162. doi:10.3189/2012AoG60A073

Schofield, O., Newman, L., Bricher, P., Constable, A., Swart, S., & Wåhlin, A. K. (2016). Moving Towards Implementation of a Southern Ocean Observing System. *Marine Technology Society Journal, 50*(3), 63-68. doi:10.4031/mtsj.50.3.8

Schwerdtfeger, W. (1984). Weather and Climate of the Antarctic. *Elsevier*.

Smith, K. L., Robison, B. H., Helly, J. J., S., K. R., Ruhl, H. A., Shaw, T. J., & ... & Vernet, M. (2007). Free-drifting icebergs: hot spots of chemical and biological enrichment in the Weddell Sea. *Science, 317*(5837), 478-482.

St-Laurent, P., Klinck, J. M., & Dinniman, M. S. (2013). On the Role of Coastal Troughs in the Circulation of Warm Circumpolar Deep Water on Antarctic Shelves. *Journal of Physical Oceanography, 43*(1), 51-64. doi:10.1175/jpo-d-11-0237.1

St-Laurent, P., Klinck, J. M., & Dinniman, M. S. (2015). Impact of local winter cooling on the melt of Pine Island Glacier, Antarctica. *Journal*

of Geophysical Research: Oceans, 120(10), 6718-6732. doi:10.1002/2015jc010709

Stammerjohn, S. E., Maksym, T., Massom, R. A., Lowry, K. E., Arrigo, K. R., Yuan, X., . . . Yager, P. L. (2015). Seasonal sea ice changes in the Amundsen Sea, Antarctica, over the period of 1979–2014. *Elementa: Science of the Anthropocene, 3*, 000055. doi:10.12952/journal.elementa.000055

Stern, A. A. (2015). Wind-driven upwelling around grounded tabular icebergs. *Journal of Geophysical Research: Oceans*, 5820-5835. doi:10.1002/2015JC010805

Stocker, T. F., Qin, D., Plattner, G. K., Alexander, L. V., Allen, S. K., Bindoff, N. L., ... , & Forster, P. (2013). Technical summary. In Climate Change 2013: The Physical Science Basis. *Contribution of Working Group I to the Fifth Assessment Report of the Intergovernmental Panel on Climate Change*, 33-115, Cambridge University Press.

Stuart, K. M., & Long, D. G. (2011). Tracking large tabular icebergs using the SeaWinds Ku-band microwave scatterometer. *Deep Sea Research Part II: Topical Studies in Oceanography, 58*(11-12), 1285-1300. doi:10.1016/j.dsr2.2010.11.004

Thoma, M., Jenkins, A., Holland, D., & Jacobs, S. (2008). Modelling Circumpolar Deep Water intrusions on the Amundsen Sea continental shelf, Antarctica. *Geophysical Research Letters, 35*(18). doi:10.1029/2008gl034939

Timmermann, R., Le Brocq, A., Deen, T., Domack, E., Dutrieux, P., Galton-Fenzi, B., . . . Smith, W. H. F. (2010). A consistent data set of Antarctic ice sheet topography, cavity geometry, and global bathymetry. *Earth System Science Data, 2*(2), 261-273. doi:10.5194/essd-2-261-2010

Torrence, C., & Compo, G. P. (1998). A practical guide to wavelet analysis. *Bulletin of the American Meteorological Society, 79*(1), 61-78.

Tournadre, J., Bouhier, N., Girard-Ardhuin, F., & Rémy, F. (2016). Antarctic icebergs distributions 1992-2014. *Journal of Geophysical Research: Oceans, 121*(1), 327-349. doi:10.1002/2015jc011178

Tournadre, J., Whitmer, K., & Girard-Ardhuin, F. (2008). Iceberg detection in open water by altimeter waveform analysis. *Journal of Geophysical Research, 113*(C8). doi:10.1029/2007jc004587

Trenberth, K. E., & Fasullo, J. T. (2013). An apparent hiatus in global warming? *Earth's Future, 1*(1), 19-32. doi:10.1002/2013ef000165

Turner, J., Orr, A., Gudmundsson, G. H., Jenkins, A., Bingham, R. G., Hillenbrand, C.-D., & Bracegirdle, T. J. (2017). Atmosphere-Ocean-Ice Interactions in the Amundsen Sea Embayment, West Antarctica. *Reviews of Geophysics*. doi:10.1002/2016rg000532

Walker, D. P., Brandon, M. A., Jenkins, A., Allen, J. T., Dowdeswell, J. A., & Evans, J. (2007). Oceanic heat transport onto the Amundsen Sea

shelf through a submarine glacial trough. *Geophysical Research Letters, 34*(2). doi:10.1029/2006gl028154

Walker, D. P., Jenkins, A., Assmann, K. M., Shoosmith, D. R., & Brandon, M. A. (2013). Oceanographic observations at the shelf break of the Amundsen Sea, Antarctica. *Journal of Geophysical Research: Oceans, 118*(6), 2906-2918. doi:10.1002/jgrc.20212

Wesche, C., & Dierking, W. (2015). Near-coastal circum-Antarctic iceberg size distributions determined from Synthetic Aperture Radar images. *Remote Sensing of Environment, 156*, 561-569. doi:10.1016/j.rse.2014.10.025

Whitworth, T. I., Orsi, A. H., Kim, S.-J., Nowlin Jr., W. D., & Locarnini, R. A. (1998). Water masses and mixing near the Antarctic Slope Front. Pp. 1–27 in Ocean, Ice and Atmosphere: Interactions at the Antarctic Continental Margin. *Antarctic Research Series, vol. 75, S.S. Jacobs and R.F. Weiss, eds, American Geophysical Union, Washington, DC.*

Visbeck, M. (2001). Deep velocity profiling using lowered acoustic Doppler current profilers: Bottom track and inverse solutions. *Journal of Atmospheric and Oceanic Technology, 19*(5), 794-807.

Wåhlin, A. K., Muench, R. D., Arneborg, L., Björk, G., Ha, H. K., Lee, S. H., & Alsén, H. (2012). Some Implications of Ekman Layer Dynamics for Cross-Shelf Exchange in the Amundsen Sea. *Journal of Physical Oceanography, 42*(9), 1461-1474. doi:10.1175/jpo-d-11-041.1

Wåhlin, A. K., Yuan, X., Björk, G., & Nohr, C. (2010). Inflow of Warm Circumpolar Deep Water in the Central Amundsen Shelf. *Journal of Physical Oceanography, 40*(6), 1427-1434. doi:10.1175/2010jpo4431.1

Young, N. W. (1998). Near-coastal iceberg distributions in East Antarctica, 50-145° E. *Annals of Glaciology, 27*, 68-74.